Lewis Acid Zeolites for Biomass Conversion: Perspectives and Challenges on Reactivity, Synthesis, and Stability

Helen Y. Luo, Jennifer D. Lewis,
and Yuriy Román-Leshkov*

Department of Chemical Engineering, Massachusetts Institute of Technology, Cambridge,
Massachusetts 02139; email: helenluo@mit.edu, jdlewis@mit.edu, yroman@mit.edu

*Corresponding author

Keywords

catalysis, biomass conversion, T-sites, pore confinement, spectroscopy,
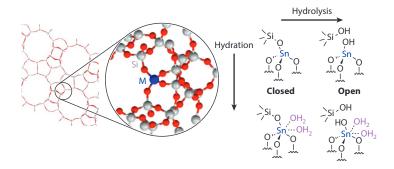Sn-Beta, Hf-Beta, Lewis acid zeolites

Abstract

Zeolites containing Sn, Ti, Zr, Hf, Nb, or Ta heteroatoms are versatile catalysts for the activation and conversion of oxygenated molecules owing to the unique Lewis acid character of their tetrahedral metal sites. Through fluoride-mediated synthesis, hydrophobic Lewis acid zeolites can behave as water-tolerant catalysts, which has resulted in a recent surge of experimental and computational studies in the field of biomass conversion. However, many open questions still surround these materials, especially relating to the nature of their active sites. This lack of fundamental understanding is exemplified by the many dissonant results that have been described in recent literature reports. In this review, we use a molecular-based approach to provide insight into the relationship between the structure of the metal center and its reactivity toward different substrates, with the ultimate goal of providing a robust framework to understand the properties that have the strongest influence on catalytic performance for the conversion of oxygenates.

INTRODUCTION

Lewis acid zeolites are versatile catalysts used for the activation and conversion of oxygenated molecules. In 1983, Eni S.p.A. researchers first discovered titanium silicalite-1 (TS-1/Ti-MFI) and the unique Lewis acid character of its tetrahedral framework sites for activating peroxides (1). Since then, many other zeolites with different topologies and heteroatoms, including Sn, Zr, Hf, Nb, and Ta, have been synthesized. In particular, the synthesis of these materials in fluoride-containing media, first reported by Corma and coworkers (2, 3), led to defect-free zeolites, such as Si-, Ti-, and Sn-Beta, with improved physiochemical properties, including higher hydrothermal stability, crystallinity, and hydrophobicity. Owing to their water-tolerant catalytic behavior, both experimental and computational studies on Lewis acid zeolites have surged in recent years in the field of biomass conversion (4, 5). Specifically, these materials have been used to catalyze oxidations, transfer hydrogenations, isomerizations, epimerizations, etherifications, acetalizations, dehydrations, aldol condensations, and Diels-Alder reactions of biomass-derived oxygenates. Several recent reviews provide comprehensive overviews on the synthesis and implementation of these Lewis acid catalysts. For example, Moliner (6) provides a detailed review of the reactivity of these materials, whereas Dapsens et al. (7) give an excellent overview of the current state of the art of synthesis and characterization of Lewis acid zeolites, with a focus on Sn-containing materials. Davis and coworkers (8, 9) offer detailed discussion of solid Lewis acid zeolites for catalyzing reactions in aqueous phases.

Despite the burgeoning number of applications of Lewis acid zeolites in biorefining, there still exist many open questions surrounding these materials. Indeed, our lack of fundamental understanding about the nature of their active sites is highlighted by the many dissonant results that have been described in recent literature reports. What makes the task of identifying the true nature of the active sites particularly challenging is the wide variation in metal site speciation that exists under reaction conditions. For instance, metals with Lewis acid character can be incorporated into the framework as a fully connected distorted tetrahedron (closed site) or have singly (open site), doubly, or triply hydrolyzed Si-O-M bonds (see **Scheme 1**). The distribution and specific geometry of these sites will depend on the zeolite topology as well as the identity of the heteroatom. Under ambient conditions, these sites are hydrated with two water molecules bound to the metal center to form a distorted octahedral geometry. In addition, metals that are not incorporated into the framework during synthesis can be deposited inside and outside the pores as extraframework oxide clusters. All of these configurations will feature intrinsically different catalytic properties, but jointly they will contribute to a net apparent behavior or catalytic activity for a given set of

Scheme 1

M-substituted zeolite Beta (*left*) and Lewis acid metal center configurations (*right*). Adapted from Luo et al. (24).

reactants, solvents, and reaction temperatures. The variety and dynamic nature of sites also make it difficult to perform meaningful characterization via ex situ spectroscopic methods. Clearly, this knowledge gap hinders our ability to unify catalytic results for zeolites synthesized by different methods and with different compositions. Understanding how to measure and control these site distributions is crucial for optimizing and ultimately predicting the catalytic performance of Lewis acid zeolites.

In this review, we use a molecular-based approach to provide insight into the relationship between the structure of the metal center and its reactivity toward oxygenated molecules in the presence of liquid-phase solvents, with the ultimate goal of providing a robust framework to understand the properties that have the strongest influence on catalytic performance. The review is divided into four main sections. First, we discuss the origin of Lewis acidity and how the electronic structure of the metal center changes upon substrate binding. Next, we compare the reactivity of different heteroatoms and offer insight derived from computational studies on their performance for different types of bond activation. We also discuss how other aspects of the zeolite framework, such as pore size, T-site geometry, and molecular connectivity, may influence the reactivity of the metal center. Third, we highlight some of the crucial characterization techniques used to study these materials and emphasize the ones that must be further optimized to determine the distribution and speciation of active sites. In the last section, we show how the stability of these materials may be tied to the changes in local structure that occur under reaction conditions. At the end of each section, we provide an outlook on the remaining challenges and potential future research directions poised to significantly advance the field. We envision that this review will serve as a didactic tool for both new and established researchers using these interesting and exciting catalysts.

LEWIS ACIDITY

A Lewis acid is modernly defined as an electron density acceptor. An archetypal example of a Lewis acid is BF_3, which has an empty 2p orbital on trivalent boron that can accept electrons from a Lewis base. The Lewis acid strength of boron can be tuned by altering the groups covalently bound to it. For instance, changing from BF_3 to BCl_3 increases the Lewis acid strength of boron because BCl_3 will have a lower-lying lowest unoccupied molecular orbital (LUMO) when compared to BF_3, which will result in a stronger bond in the acid-base pair adduct. In a related way, tetrahedrally coordinated metals (M^{4+}) built into a silica framework can act as Lewis acids. The Lewis acid character arises from the partial positive charge on the metal atom that is formed when valence electrons of the metal covalently bind with adjacent framework oxygen atoms. The metal site can accept electron pairs from reactants without inducing a charge imbalance in the framework, and this can lead to chemical activation of substrates with electron-rich groups. The properties of this activation depend heavily on the identity of both the heteroatom and the reagent, which affect the electronic structure, flexibility, and stability of the resulting adduct.

Origin of Lewis Acidity

To illustrate the complex interaction between substrate and catalyst, we provide an in-depth discussion of the activation of carbonyl functional groups by Lewis acid zeolite catalysts. The major interaction between the Lewis acid and substrate involves electron density shifting from the p_z and p_y orbitals of the carbonyl oxygen atom and from the carbonyl $\pi(C=O)$ bond to the catalyst LUMO (10). The nature of the catalyst's LUMO depends on the identity of the metal (see **Figure 1**). For Sn it is the $\sigma^*(Sn-O)$ orbitals of the cluster, whereas for Ti, Zr, and Hf it is the $d_z{}^2$
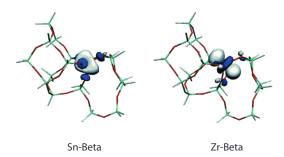
Sn-Beta   Zr-Beta

Figure 1

Lowest unoccupied molecular orbital (LUMO) of Sn-Beta and Zr-Beta active sites. Reprinted with permission from Reference 68, ©2006 American Chemical Society.

atomic orbitals of the heteroatom. Back-donation of electron density from the highest occupied molecular orbital (HOMO) of the catalyst (i.e., the lone pairs on the oxygen atoms neighboring the framework metal) to the LUMO of the organic molecule [i.e., the antibonding π^*(C=O) orbital on the carbonyl] is observed with some systems. The ability for back-donation depends on the orbital overlap and energy gap between the substrate LUMO and the catalyst HOMO that are generated based on the particular nature of both the substrate and the metal. Theoretical studies have shown that the Mulliken charges of the Lewis acid metal centers in zeolites increase upon the adsorption of NH_3 (11). This implies that the additional electron density transferred from the coordination of an electron-rich group cannot be fully accepted by the metal itself and is transferred onto the neighboring oxygen atoms, resulting in delocalization of the catalyst LUMO. This effect is larger for Sn-containing zeolites owing to the nature of their σ^*(Sn-O) LUMO (10, 12) and results in a larger partial negative charge on the neighboring oxygen atoms upon accepting electron pairs (e.g., from a carbonyl group).

The size of the heteroatom and its flexibility in the zeolite framework are additional factors that affect Lewis acidity. Introduction of a heteroatom results in significant deviation from the O-Si-O tetrahedron angles and is thermodynamically disfavored. The magnitude of this deviation varies by metal type and framework location. For example, the mean square deviation from a regular tetrahedron for the substitution of a heteroatom at the T2 site in zeolite Beta was found to be 1.8 for Ti, 3.4 for Sn, and 2.3 for Zr (13). Li et al. (12) showed with a hybrid quantum mechanics/molecular mechanics (QM/MM) study that the geometric distortion of the zeolite framework surrounding the metal atom is a significant contributor to the total activation energy for the isomerization of glucose. Specifically, this distortion adds approximately 15 kcal/mol to the total activation energy calculated for Sn-Beta. They observed that larger metal atoms with higher polarizability allow for greater structural flexibility and result in a lower energy penalty.

Quantifying Lewis Acidity

Quantifying Lewis acidity is difficult owing to the lack of a single reference to determine the affinity scale (14). The hard-soft acid-base theory uses thermodynamic and kinetic arguments based on charge and polarizability to rank molecular species. Unfortunately, this metric is insufficient to accurately describe Lewis acidity in zeolite materials. Several computational and experimental studies have tried other scales to quantify the Lewis acidity of the framework cluster to predict reactivity. Yang et al. (11) performed a comprehensive density functional theory (DFT) study on M^{4+} substituted zeolites in the MFI framework. They investigated a series of possible descriptors for Lewis acidity including LUMO energies, Fukui functions, absolute electronegativity, and
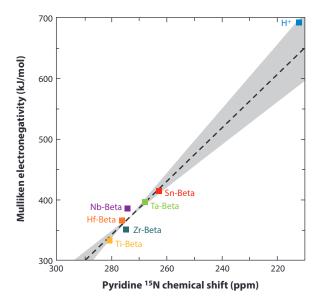
Figure 2

Experimental Mulliken electronegativity versus pyridine ^{15}N magic angle spinning nuclear magnetic resonance chemical shift (W.R. Gunther, V.K. Michaelis, R.G. Griffin, and Y. Román-Leshkov, manuscript submitted).

absolute hardness. It was found that none of these descriptors, which depend only on the zeolite itself, correlated with the Lewis acidity observed experimentally. Instead, the calculated adsorption energy of ammonia (NH_3) could more accurately predict the Lewis acid strength order of MFI zeolites: Si $\ll$ Ge $<$ Ti $<$ Pb $\leq$ Sn $\leq$ Zr. Li et al. (15) came to an analogous conclusion when a similar Lewis acid strength order of Ti $<$ Zr $\leq$ Sn was found when computationally evaluating COE-4 (delaminated FER topology) zeolites using probe molecule adsorption energies. Although several theoretical studies have been conducted on the topic (16, 17), few comprehensive experimental studies quantify Lewis acidity across different heteroatoms. To this end, Gunther et al., using magic angle spinning (MAS) nuclear magnetic resonance (NMR) of ^{15}N pyridine adsorbed on M-Beta zeolites, found that the experimentally observed ^{15}N chemical shift provides a scale for Lewis acidity that correlates well with Mulliken electronegativities and pyridine adsorption energies, as seen in **Figure 2** (W.R. Gunther, V.K. Michaelis, R.G. Griffin, and Y. Román-Leshkov, manuscript submitted). The trend of Lewis acid strength agrees with previous computational studies: Ti $<$ Hf $\leq$ Zr $<$ Nb $<$ Ta $<$ Sn.

Correlating Heteroatom Identity and Catalytic Activity

Experimentally, only a loose correlation is observed between catalytic activity and Lewis acid strength for various reactions. **Table 1** summarizes the relative activity of different zeolites for many classes of reactions. For each class of reactions, the specific substrates and conditions are reported, and where possible, the activities of the different materials are compared using initial rates. Titanium-containing zeolites, such as Ti-MFI and Ti-Beta, catalyze the epoxidation of linear alkenes with aqueous H_2O_2 (18, 19), but Zr- and Sn-containing zeolites show no activity for this reaction (10). In contrast, Sn-containing zeolites are active for the Baeyer-Villiger (BV) oxidation of cyclic ketones and aromatic aldehydes with H_2O_2, whereas Zr-Beta exhibits five times

Table 1 Order of reactivity for different heteroatom-incorporated zeolite catalysts for various reactions and substrates

Nature of transformation	Substrate(s)	Product	Conditions	Material activity order	Reference
Epoxidation	Octene	Epoxyoctane	H_2O_2, methanol, 333 K	Zr-Beta[e] ≈ Sn-Beta[e] < Ti-Beta	10[a]
	Cyclohexene	Epoxycyclohexane	*Tert*-butyl hydroperoxide, octane, 333 K	Ti-MFI[e] < Ti-DZ-1[c] < Ti-UCB-4[d]	32[a,b]
Oxidation	Diphenyl sulfide	Diphenyl sulfoxide/ diphenyl sulfone	H_2O_2, acetonitrile	Sn-Beta[e] < Ti-Beta ≈ Zr-Beta	10[a]
Baeyer-Villiger oxidation	Cyclohexanone	Caprolactone	H_2O_2, dioxane, 363 K	Ti-Beta[e] < Zr-Beta < Sn-Beta	10[a]
	2-Adamantanone	2-Adamantanone lactone	H_2O_2, dioxane, 348 K	Si-DZ-1[c] < Nb-DZ-1 < Zr-DZ-1 < Ti-DZ-1 < Ta-DZ-1 < Hf-DZ-1 < Sn-DZ-1 < Sn-Beta	32[a,b]
				Sn-MFI < Sn-MFI-nanosheets ≈ Sn-MCM-41 < Sn-Beta	33[a]
			H_2O_2, dioxane, 363 K	(Sn-MCM-41 < Sn-Beta)[f]	56[a]
Intramolecular hydride shift	Glucose	Fructose	Water, 413 K	Ti-MFI[e] < Ti-MCM-41 < Sn-MCM-41 < Ti-Beta < Sn-Beta	20
			Water, 358 K	Sn-MFI < Ti-Beta < Sn-Beta	71
			Water, 353 K	Sn-MFI[e] ≈ Sn-SBA-15[e] < Sn-MCM-41 < Sn-Beta	58
	Lactose	Lactulose	Water, 373 K	Ti-Beta < Sn-Beta	35[a]
	Glyceraldehyde	Dihydroxyacetone	Water, 363 K	Ti-Beta < Zr-Beta < Sn-Beta	21[b]
Dehydration + esterification + intramolecular hydride shift	Dihydroxyacetone	Methyl lactate	Methanol, 353 K	Si-Beta[e] < Sn-MFI ≈ Sn-SBA-15 ≈ Sn-MCM-41 < Sn-Beta	58
				Si-Beta[e] ≈ Al-Beta[e] ≈ Ti-Beta[e] ≈ Zr-Beta[e] < Sn-Beta	118
	Dihydroxyacetone	Lactic acid	Water, 398 K	Si-Beta[e] < Al-Beta ≈ Ti-Beta < Zr-Beta < Sn-Beta	118
			Water, 363 K	Sn-Beta[e] ≈ Sn-MFI	61
Intramolecular carbon shift	Glucose	Mannose	1:4 Sodium borate: sugar, water, 358 K	Si-Beta[e] < Sn-MFI < Ti-Beta < Sn-Beta	71
			Methanol, 353 K	Sn-MFI[e] < Sn-SBA-15 < Sn-MCM-41 < Sn-Beta	58

(*Continued*)

Table 1   (*Continued*)

Nature of transformation	Substrate(s)	Product	Conditions	Material activity order	Reference
Intermolecular hydride shift	Cyclohexanone	Cyclohexanol	2-Butanol, 373 K	Ti-Beta < Zr-Beta < Sn-Beta	10, 68[a]
				Si-Beta[e] < Ti-Beta < Al-Beta < Sn-Beta	119
				Si-Beta[e] ≈ B-Beta[e] ≈ V-Beta[e] < Ti-Beta < Al-Beta < Sn-BetaSn-MCM-41< Sn-Beta	14
	Benzaldehyde	Benzyl alcohol	2-Butanol, 373 K	Ti-Beta[e] < Sn-Beta < Zr-Beta	10[a]
	4-*Tert*-butylcy-clohexanone	4-*Tert*-butylcy-clohexanol	2-Propanol, 355 K	Si-Beta[e] ≈ Al-Beta[e] <Ti-Beta < Sn-Beta ≈ Zr-Beta	23
	Methyl levulinate	γ-Valerolactone	2-Butanol, 393 K	Al-Beta[e] < Ti-Beta < Sn-Beta < Zr-Beta < Hf-Beta	24, 111[a]
	Crotonaldehyde	Crotyl alcohol	Ethanol, 473 K	Zr-MCM-41 ≪ Zr-Beta	120[a]
Intermolecular hydride shift + etherification	5-(Hydroxy-methyl)furfural	2,5-Bis(ethoxy-methyl)furan	Ethanol, 393 K	Si-Beta[e] ≈ Ti-Beta[e] ≈ Nb-Beta[e] ≈ Ta-Beta[e] ≈ Sn-MCM-41[e] < Zr-MCM-41 < Sn-Beta < Zr-Beta < Hf-Beta	25
Acetalization	Glycerol + acetone	Solketal	*Tert*-butanol, 353 K	Sn-TUD-1 ≈ Zr-TUD-1 < Hf-TUD-1(Hf-TUD-1 < Zr-TUD-1 < Sn-TUD-1)[f]	121
Aldol condensation	Dihydroxyacetone + paraformalde-hyde	α-Hydroxy-γ-butyrolactone	Dioxane, 20 bar, 433 K	Ti-Beta ≈ Hf-Beta ≈ Zr-Beta < Sn-Beta ≈ Sn-MCM-41 ≈ Sn-MFI	22
	Benzaldehyde + acetone	Benzalacetone	Toluene, 363 K	Si-Beta[e] ≈ Al-Beta[e] ≈ Ti-Beta[e] < Sn-Beta < Zr-Beta ≈ Hf-Beta	26
Diels-Alder	Furan derivative + ethylene	*p*-xylene derivative	Dioxane, 70 bar, 363 K	Ti-Beta[e] < Sn-MFI ≈ Sn-MCM-41 < Zr-Beta < Sn-Beta	122

[a]Initial rates.
[b]Postsynthetic material.
[c]Delaminated MWW framework topology.
[d]Delaminated SSZ-70 framework topology.
[e]Nearly no activity.
[f]Normalized by titrated acid sites.

lower initial rates, and Ti-Beta shows no activity. The key difference between these two types of reactions is the order in which the reactants are activated. For epoxidations, H_2O_2 must first adsorb onto the Lewis acid center to form an active hydroperoxo species. It was found that the most important parameter of the system is the positive charge on the oxygen atom in H_2O_2 that is bound to the metal center, and this is maximized for Ti-Beta, which has the lowest-energy LUMO out of the three metals studied (10). For BV oxidations, the carbonyl group is first activated by the metal center and then forms a Criegee intermediate with H_2O_2, implying that the Lewis acid character of Sn is better suited for activating the carbonyl group, making the carbon more prone to attack by the peroxide. Similarly, Sn-containing zeolites tend to show higher activity

for reactions involving the initial activation of carbonyl compounds, such as the isomerization of glucose to fructose (20), isomerization of glyceraldehyde to dihydroxyacetone (DHA) (21), and C-C coupling between DHA and formaldehyde (22), when compared to Ti-containing zeolites. However, for the Meerwein-Ponndorf-Verley (MPV) reduction using alcohol hydrogen donors via a six-membered ring transition state where both reactants are bound to the metal center, Zr- and Hf-Beta show either higher or similar activity to that of Sn-Beta, whereas Ti-Beta shows drastically lower activity (23, 24). The exact order of reactivity of the different metals for the MPV reaction depends highly on the substrates and solvents used. For example, the MPV reduction of cyclohexanone has the highest rates over Sn-Beta by a factor of 4.5, but if the reactant is switched to benzaldehyde, Zr-Beta has the highest rates (10). Similarly, for the combined MPV reduction and etherification of 5-(hydroxymethyl)furfural (HMF) to 2,5-bis(ethoxymethyl)furan (25) and the cross-aldol condensation of aromatic aldehydes and acetone (26), both featuring a dual-binding transition state, we observe higher reactivity over Hf- and Zr-Beta and lower reactivity over Sn-Beta.

Outlook

Table 1 shows that Ti-zeolites are most active for epoxidations; Sn-zeolites are most active for BV oxidation and intramolecular carbon and hydride shifts; and Zr- and Hf-zeolites are equally or more active for intermolecular hydride shifts, etherifications, and aldol condensations. It is important to note, however, that most of the comparisons featured in **Table 1** were based on rates normalized by total metal content and do not account for possible extraframework or inactive metal species. Additionally, most data were obtained in batch reactors without applying criteria to test for mass transfer limitations, and only a small portion of the studies provided the initial reaction rates. In general, high conversion data are not as accurate for comparing catalytic activity unless reaction orders are calculated.

Performing rigorous kinetic studies is essential to compare the behavior of different catalysts. The importance of kinetic studies is highlighted in work conducted by our group on the liquid-phase MPV reduction of methyl levulinate to γ-valerolactone (GVL) over M-Beta zeolites using flow reactors operating under differential conditions in the absence of mass transfer limitations. It was found that the apparent activation energies for Zr-, Hf-, and Sn-Beta were all approximately 52 kJ/mol (24). The difference in activity between these catalysts was instead attributed to entropic effects associated with vastly different pre-exponential factors, with the order of activity of Sn < Zr < Hf. These results suggest that factors other than intrinsic Lewis acid strength, such as geometric configurations within the pores, also play an important role in determining catalytic activity.

Understanding the Lewis acidity of active sites in Lewis acid zeolites is essential for designing materials to catalyze particular reactions. From the studies discussed above, we conclude that any Lewis affinity scale developed to rank these materials will depend heavily on the conditions and substrates employed. Therefore, the use of probe molecules in conjunction with spectroscopic techniques will be more beneficial for predicting activity. Clearly, the type of heteroatom alone cannot account for all the observed differences in reactivity, and there are further effects of the zeolite environment. Rigorous kinetic tests are essential to highlight subtle, but important, differences among catalysts. In addition, one must not forget that reactivity comparisons based on turnover frequencies (TOFs) can be reliable only when the number of active sites is accurately quantified. These parameters are discussed in the next sections.

ZEOLITIC ENVIRONMENT

Effects on reactivity imposed by the zeolite environment can be divided into local factors that influence the metal center directly and extended factors that influence the conformation and diffusion of solvents and substrates within the pores. Pore size effects have been extensively reviewed in the literature and are the reason zeolites are valued for their shape selectivity (27). We only briefly discuss some of the extended factors as they relate specifically to performance of Lewis acid centers. We focus in more detail on the local factors that influence the flexibility and electronic properties of the metal center and bound transition states, such as T-site location and local defects on or near the active site (open/closed sites).

Extended Properties

For applications involving zeolite catalysts, it is well known that the pore and cage sizes must be carefully selected to allow access of the reactants and products to active sites. This is no different for Lewis acid zeolites, where many studies have shown the importance of site accessibility for converting bulky reactants (28, 29). Often it is desirable to tune crystal size or introduce mesoporosity in Lewis acid zeolites to allow better diffusion to and from active sites and decrease the chance of pore blockage owing to deposition of side products. To this end, Rimer and coworkers (30, 31) have shown that zeolite growth modifiers are capable of modulating zeolite crystal structure. Ouyang et al. (32) show that delaminated Sn-DZ-1, an MWW framework material with Sn postsynthetically incorporated into surface-accessible sites, has higher activity for the BV oxidation of 5-bromo-2-adamantanone with H_2O_2 than Sn-Beta. The TOF per Sn site is 688 h^{-1} for Sn-DZ-1 compared to 366 h^{-1} for Sn-Beta. However, if the substrate is 2-adamantanone, which is not as sterically hindered in 12-ring pores as its brominated derivative, then the TOF is higher for Sn-Beta (1,963 h^{-1}) compared to Sn-DZ-1 (866 h^{-1}). Similar benefits of site accessibility were found for hierarchical Sn-containing MFI zeolite nanosheets (33, 34). In addition to controlling activity through steric effects, the zeolite environment can control the partitioning of solvent molecules. Water and other highly polar molecules will bind with Lewis acids and compete with reactants, effectively lowering the catalyst activity. Hydrophobic zeolites have the ability to keep bulk water out of the channels, even in aqueous conditions (3). Gounder & Davis (35) showed that defect-free Ti-Beta synthesized in fluoride media has order of magnitude–higher rate constants for glucose isomerization in both water and methanol compared with Ti-Beta synthesized in hydroxide media. Notably, hydrophobic Lewis acid zeolites are able to selectively adsorb sugars from aqueous solutions. Bai et al. (36) found through Monte Carlo simulations that glucose is preferentially shuttled into zeolite pores owing to a large entropic gain of approximately 90 J/(mol K) from desolvation of the sugar's hydration shell.

T-Sites and Local Geometry of the Active Site

The distinct geometry of T-sites within or between topologies will influence the local configuration and, consequently, the acidity of the metal center. An early DFT study by Sastre & Corma (37) showed that the LUMO energy depends on the T-site's Ti-O-Si angles in Ti-zeolites, making Ti-Beta a stronger Lewis acid than Ti-MFI. In addition, the relative substitution energies for different T-sites in the same topology are different enough thermodynamically to influence the distribution of metal centers. Computational (13, 38) and extended X-ray absorption fine structure (EXAFS) spectroscopy studies (39) suggest that Sn preferentially occupies T-sites in the four-membered rings in Beta zeolites (**Figure 3**). These sites are designated as T1/T2 by Newsam
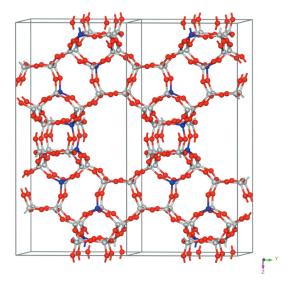
Figure 3

The zeolite Beta framework with T2 sites highlighted in blue using the notation from Newsam et al. (40).

et al. (40) or as T5/T6 by the International Zeolite Association Structure Commission (41). It has also been hypothesized that Sn can form paired sites across six-membered rings in Beta topology, which may enhance the Lewis acidity compared with other framework topologies (13, 39). Computational studies (42–49), as well as experimental investigations using neutron diffraction (50–52) and synchrotron radiation powder X-ray diffraction (PXRD) (53, 54) of Ti-MFI, have not shown consistent results on Ti siting. Deka et al. (49) proposed that these experimental discrepancies are due mainly to kinetic effects caused by differences in synthesis conditions between research groups.

Confinement effects enforced by the pore structure play a major role in stabilizing transition states for certain reactions. Sn^{4+} sites grafted on silica and Sn^{4+} sites incorporated into amorphous nonmicroporous MCM-41 have significantly lower activity than Sn-zeolites for MPV reductions and BV oxidations on a per-site basis (55–57). Experimentally, it is difficult to separate the effects of pore size confinement from T-site effects in zeolites with the same heteroatom but with different topology. Some of these comparisons are featured in **Table 1**. Osmundsen et al. (58) found that Sn-Beta had approximately 10 times the activity of Sn-MFI, Sn-MCM-41, and Sn-SBA-15 for DHA conversion to methyl lactate in methanol at 313 K. These molecules do not suffer from diffusion limitations in 10-ring or larger pores, so the observed differences may depend more on the active site distribution and T-site geometry than on confinement effects (59). Similarly, Ouyang and coworkers (32) found that Sn-DZ-1 (delaminated MWW) is 2.4 times more active than Sn-UCB-4 (delaminated SSZ-70, medium pore zeolite) for the BV oxidation of 2-adamantanone. This effect is inverted for the epoxidation of 1-octene with Ti-DZ-1, which is 2.6 times less active than Ti-UCB-4. Other systems show a more obvious contribution of pore confinement on the transition state. De Clercq et al. (60) show that for the conversion of tetrose sugars to four-carbon α-hydroxy acid esters with tin-containing catalysts, the selectivity shifts from the bulkier methyl-4-methoxy-2-hydroxybutanoate (MMHB) to the smaller methyl vinyl glycolate upon decreasing the pore size. For mesoporous Sn-SBA-15 and Sn-MCM-41, the product selectivity to MMHB is approximately 85% and 87%, respectively, at 363 K. These values decrease to 63% and 41% when using Sn-Beta and Sn-MFI, respectively. A careful kinetic analysis revealed that although

the activation energy to form MMHB in Sn-Beta is 37 kJ/mol lower than that of the mesoporous materials, the pre-exponential factor is five orders of magnitude smaller, leading to drastically lower apparent rate constants for the desired reaction at 433 K. Analysis of the entropies revealed that the penalty in the microporous materials was 96 J/(mol K) higher for forming the transition state associated with MMHB than the one for methyl vinyl glycolate owing to steric hindrance inside the pores. Lewis et al. (26) also observed confinement effects in the aldol condensation of acetone and benzaldehyde, where Hf-, Zr-, and Sn-Beta catalyzed the single condensation product benzalacetone with a selectivity >90%, whereas nonporous MgO achieved only 42% selectivity owing to coproduction of the double condensation product dibenzalacetone. For some reactions, differences in T-sites and pore size do not seem to make a significant difference. Lew et al. (61) saw very similar conversion and selectivity for Sn-Beta and Sn-MFI for the conversion of DHA to lactic acid in water, and Van de Vyver et al. (22) reported very similar activity for Sn-Beta, Sn-MFI, and Sn-MCM-41 for the multistep conversion of DHA and formaldehyde to α-hydroxy-γ-butyrolactone (HBL).

Molecular Connectivity of the Metal Center

As discussed in the introduction, molecular connectivity of the metal center can assume several states from fully closed sites to triply hydrolyzed defect sites. There is theoretical and experimental evidence for the presence of open sites for Ti-, Sn-, and Zr-containing zeolites (62, 63). This connectivity can affect the site flexibility, which can reduce the energy required for geometric distortion during the formation of a transition state. Additionally, the metal hydroxy group and the adjacent silanol group of an open site are known to participate in reaction mechanisms. Experiments using sodium exchange and theoretical mechanistic studies show evidence that the open site is more active for the epoxidation of alkenes over Ti-MFI (64–66). Boronat et al. (67) show that the number of open sites in Sn-Beta, measured with acetonitrile adsorption Fourier transform infrared spectroscopy (FTIR), correlates linearly with the initial rates for the BV-oxidation of adamantanone. DFT calculations on the proposed transition states show that the open site's metal hydroxy group is required to bind H_2O_2. This same correlation is found for the MPV reduction of cyclohexanone with 2-butanol over both Sn- and Zr-Beta (68). However, in this case, the metal hydroxy group is thought to allow deprotonation of the alcohol, forming a bound water molecule. Sushkevich et al. (69) performed a similar study that correlated initial rates for ethanol condensation to the number of open sites in Zr-Beta determined by CO adsorption coupled with FTIR. Their DFT calculations suggest that stronger acidity and greater flexibility of the open site are responsible for the higher reaction rate.

The importance of molecular connectivity has been studied extensively for the isomerization and epimerization of glucose with Sn-Beta (63, 70). Gunther et al. (71, 72) demonstrated that although the activation barriers for epimerization and isomerization are virtually identical for reactions catalyzed by Sn-Beta, the presence of substoichiometric amounts of borate induced a drastic selectivity shift in favor of epimerization over isomerization. Similarly, Bermejo-Deval et al. (73) hypothesized that exchanging Sn-Beta with Na^+ increases epimerization selectivity over isomerization because the active site for isomerization is an open site, and exchanging Na^+ onto the adjacent silanol modifies the site properties needed to carry out the isomerization reaction. This was further supported by Brand et al. (74) using tin silsesquioxanes as molecular analogs to framework Sn-Beta sites. They showed that octahedral tin sites with an adjacent silanol group favored the isomerization of glucose to fructose through a 1,2-hydride shift, whereas removing the silanol increased the selectivity to mannose through a 1,2-carbon shift. In contrast, Wolf et al. (75) suggested that both open and closed sites are active for isomerization based on [119]Sn dynamic

nuclear polarization (DNP) MAS NMR of postsynthetically synthesized Sn-Beta with different relative ratios of open and closed sites. Theoretical studies have attempted to clarify the significance of open versus closed configurations, but the results have depended heavily on the chosen glucose binding modes and the theoretical techniques used (76). For example, Yang et al. (13) found no significant difference in the reactivity of open and closed sites, but they concluded that a nearby silanol nest is beneficial for activating sugar intermediates. However, Li et al. (12) found that the open site is intrinsically more active owing to an increase in flexibility of the metal center. Others have claimed the importance of open site silanols (77) and coordinated water molecules (78) for assisting in proton transfer during ring opening. We note that the possible roles of sites that are doubly or triply hydrolyzed were not addressed in any of these studies. These conflicting results highlight the need for further characterization (particularly under reaction conditions) and theoretical studies to determine the exact role of open and closed sites in the catalytic cycle.

Effects of Synthesis Techniques

The distribution of metal sites in Lewis acid zeolites can be heavily influenced by the synthetic method used to introduce heteroatoms into the zeolite topology. Differences can arise from varying extraframework metal content, T-site location, molecular connectivity, concentration of defect sites, and crystal morphology. In particular, the type of metal salt used as a precursor in hydrothermal syntheses heavily influences the framework content and catalytic activity of the final product (79, 80). Recently, many groups have reported dry-gel or postsynthetic methods for metal incorporation in zeolite Beta (21, 81, 82). These methods can often incorporate a higher metal content into the zeolite framework compared with the hydrothermal method. This leads to higher yields normalized by total catalyst mass for certain reactions, but lower TOFs when normalized by metal content at loadings above 3–5% (83–85). For example, Hammond et al. (86) show for Sn-Beta made by solid-state postsynthetic modification of dealuminated Beta that the lower TOFs for glucose isomerization are due primarily to a higher fraction of extraframework species, which are present at tin contents above 5 wt%. Careful characterization of the postsynthetic 2 wt% Sn-Beta using ^{119}Sn MAS NMR, EXAFS, and acetonitrile adsorption coupled with FTIR seems to indicate a very similar distribution of active sites to that in hydrothermally (HT) synthesized Sn-Beta. However, current characterization techniques are unable to confidently distinguish differences in T-site location and molecular connectivity of these materials. Dealumination followed by postsynthetic grafting can populate many different T-sites (87) and may also lead to more open sites owing to the high defect density in the material. In a comprehensive study, Dijkmans et al. (88) found that the performance of Sn-Beta depended heavily on the synthesis method, the type and amount of Sn precursor, and the type of probe reaction used. HT-synthesized Sn-Beta was far more active for the isomerization of glucose to fructose in water, with a TOF of 306 h^{-1} compared to a TOF of 152 h^{-1} for Sn-Beta made by isopropanol-assisted grafting of Sn(IV) chloride pentahydrate onto dealuminated Beta (IPA-graft). However, for the MPV reduction of cyclohexanone with 2-butanol, the TOF of IPA-graft Sn-Beta was higher at 96 h^{-1} compared to a TOF of 78 h^{-1} for HT Sn-Beta. This inversion was also seen for the BV oxidation of cyclohexanone using H_2O_2. Careful characterization of the Sn site and the proximate silanol groups using X-ray absorption spectroscopy (XAS), diffuse-reflectance UV/visible (DRUV) spectroscopy, and temperature programmed reduction revealed differences in the geometry and electronic properties of HT Sn-Beta and IPA-graft Sn-Beta (89) that may contribute to transition state stabilization. Clearly, variations in local site geometry and connectivity as well as the extended pore environment obtained from different synthesis techniques can drastically affect reactions that are sensitive to these changes.

Outlook

From the bulk characteristics and pore structures to the local geometry and molecular connectivity at the site level, the section above showed that many properties of the zeolite's environment influence catalytic activity for particular reactions. To determine concrete relationships between structure and activity, it is essential to deconvolute these effects. Future work should focus on performing careful kinetic studies to parse out the different contributions to catalytic activity. For these comparisons to be meaningful, it is critical to always establish a benchmark in studies comparing multiple materials. For example, the activity of HT Sn-Beta for glucose isomerization in water (82, 88, 90) featuring a $TOF = 100–120$ (mol glucose) (mol Sn)$^{-1}$ h^{-1} at 368–383 K when using an initial concentration of (mol glucose) (mol Sn)$^{-1} = 100$ has been reproduced by several research groups; hence, it can be used as a reliable benchmark. As more alternative synthesis techniques are developed, the consistent use of benchmark materials should be complemented by including comparisons on a metal content or acid site count basis rather than total catalyst mass, so that more relevant conclusions can be drawn about the nature of the active centers. To this end, more precise characterization of the active center and its local environment through spectroscopic techniques is needed. Recent advances in this area are discussed in the following section.

SPECTROSCOPY

Given the variety of structural factors that can affect the activity of Lewis acidic metal centers, characterization techniques that can probe the distribution of sites are crucial for understanding properties that dictate performance in catalytic reactions. These techniques can be separated into two categories: direct detection of the metal center and indirect detection using probe molecules. Dapsens et al. (7) provide a brief overview of many of these techniques with a focus on Sn-containing zeolites. We provide a list of techniques in **Table 2**, including some of the advantages and disadvantages for each method. Many techniques have focused on probing metal coordination and distinguishing between framework and extraframework species. Major challenges for spectroscopic methods include (*a*) probing and quantifying reliably the connectivity of the active sites, (*b*) identifying variations in T-site distribution, and (*c*) refining detection methods that can be used for all heteroatoms.

Direct Detection of the Metal Center

Direct detection techniques have typically focused on determining the coordination of framework heteroatoms and assessing the extent of extraframework MO_x species. The most commonly used technique is DRUV spectroscopy, which can give a quick qualitative assessment of the types of species present in a sample. An adsorption band of approximately 200–220 nm is assigned to the charge transfer from O^{2-} to M^{4+} tetrahedral framework sites for Sn- (90) and Ti-containing (91) zeolites. Octahedral bulk oxide or oligomeric species typically have adsorption bands in the 240–300-nm range. Semiquantitative data can be obtained by converting the reflectance to the Kubelka-Munk function, which can be linearly correlated with the concentration of a species. The wide variety of different band shapes and intensities of DRUV spectra reported by different groups for the same materials have led to confusion and data misinterpretation. Many of these differences are due to inconsistent sample preparation, lack of a proper background standard, and improper diffuse-reflectance instrumentation. However, when done properly, this method can provide valuable insight into the distribution of framework and extraframework species. Dijkman et al. (88) provide an excellent example in which they show that the intensity of the extraframework

Table 2 Characterization techniques for probing Lewis acid zeolites[a]

Technique	Heteroatom	Information gained	Disadvantages	Reference
Diffuse reflectance UV/visible spectroscopy	Hf, Sn, Ti, Zr, Nb, Ta, V	Coordination	Low signal to noise Inconsistent reports in literature	21, 25, 28, 84, 88, 99, 109, 123–126, 89, 91, 108
Direct metal center MAS NMR spectroscopy	^{119}Sn	Coordination Hydration Connectivity Quantification (T-site)	Requires long acquisition times or ^{119}Sn enrichment DNP methods not quantitative	63, 75, 86, 90, 92, 93, 110, 127–129
Mössbauer spectroscopy	^{119}Sn	Oxidation state	Cannot distinguish between tetrahedral Sn and SnO_2	75, 125, 130–132
X-ray adsorption (XANES, EXAFS) spectroscopy	Sn, Ti, Ta, Nb, (All)	Coordination T-site location Connectivity	Requires synchrotron facility Low signal to noise Requires extensive modeling	39, 62, 86, 89, 94, 109, 133, 134
Synchrotron powder X-ray diffraction	Ti	Coordination T-site location	Requires synchrotron facility	53, 54
X-ray photoelectron spectroscopy (XPS)	Sn, Zr, (All)	Substrate-Sn interactions Oxidation state (Coordination)	Inconsistent reports in literature	29, 71, 83, 84, 134, 135
Neutron diffraction	Ti, Fe	T-site location	Inconsistent reports in literature Requires extensive modeling	50–52
Raman spectroscopy	Ti, Sn	Coordination	Detection limit for MO_2 unknown M-O-Si vibration not visible	81, 94, 135
Electron microscopy (SEM, TEM, STEM)	Sn, (All)	Coordination	Can detect only large MO_x particles	79, 108
Direct FTIR spectroscopy	Ti, Sn	Coordination	M-O-Si vibration not visible	89, 94, 136, 137
Temperature programmed desorption	Sn, (All)	Coordination Acidity Quantification		99
MAS NMR probe molecules				
Trimethylphosphine, Trimethylphosphine oxide	Al, (All)	Acidity Coordination (Hydration) (T-site) (Connectivity) (Quantification)	Not well studied in the literature	101, 138
Pyridine	Sn, Hf, Ti, Zr, Nb, Ta	Acidity Coordination Quantification (Connectivity)	Not well studied in the literature	18
FTIR probe molecules				
Deuterated acetonitrile	Sn, Ti, Zr, Hf, (All)	Coordination Connectivity	Inconsistent reports in literature	67, 82, 84, 86, 88, 99

(*Continued*)

Table 2 (*Continued*)

Technique	Heteroatom	Information gained	Disadvantages	Reference
Cyclohexanone	Sn, Ti, (All)	Coordination		14, 88, 109, 118, 119, 139
Pyridine 2,6-Di-*tert*-butylpyridine	All	Coordination Acidity Quantification		29, 82–85, 88, 100
Carbon monoxide	Zr, (All)	Coordination Connectivity Quantification	Not well studied in the literature	69, 100, 115

[a]Parentheses indicate potential heteroatoms and information that can be gained in future studies.

Abbreviations: DNP, dynamic nuclear polarization; EXAFS, extended X-ray absorption fine structure; FTIR, Fourier transform infrared spectroscopy; MAS, magic angle spinning; NMR, nuclear magnetic resonance; SEM, scanning electron microscopy; TEM, tunneling electron microscopy.

Sn species at 255 nm increases as the Sn content increases above 2 wt% for postsynthetically grafted Sn-Beta. They also show that the intensity of the framework Sn signal at 200 nm increases up to 2 wt% Sn and then stays constant (see **Figure 4a**). Their method ensures proper drying of samples and background correction using dealuminated Beta zeolite to isolate only the Sn-related signals and uses the proper instrumentation for operating in this spectral region. Unfortunately, DRUV cannot detect the small amount of extraframework SnO_2 particles that are observed on almost all Sn-Beta samples analyzed by scanning electron microscopy (SEM) (79). Because SEM and tunneling electron microscopy can detect MO_x particles in zeolite samples, but cannot detect oligomeric extraframework species, their use provides only qualitative results.

MAS NMR is a reliable method for probing and quantitating framework and extraframework species, as long as the nuclei of interest are amenable to NMR analysis. For instance, Sn-containing materials can be analyzed using ^{119}Sn MAS NMR but require enrichment of the ^{119}Sn isotope (natural abundance ~8.6%) to avoid prohibitively long acquisition times. Nonetheless, MAS NMR provides unparalleled information about the environment surrounding the metal centers with high resolution. In tin-containing zeolites, extraframework SnO_2 species exhibit a sharp signal at −604 ppm, whereas tetrahedral framework Sn sites have a distribution of signals in the −420 to −450 ppm range when dehydrated and in the −650 to −730 ppm range when hydrated, as shown in **Figure 4b**. Spectra acquired with direct excitation can be integrated to calculate the site distribution; however, care must be taken to ensure acquisition parameters, such as relaxation times, are appropriately configured to obtain quantitative spectra. Advanced NMR methods can provide more information about the coordination and T-site distribution. Bermejo-Deval et al. (73) showed that both Na^+ exchange and ammonia adsorption specifically titrate a resonance at −423 ppm, which most likely corresponds to a singly hydrolyzed open site. ^1H-^{119}Sn cross-polarization (CP) MAS NMR experiments after ammonia adsorption indicated that there was no proton source near the resonance at −443 ppm, which is believed to be the closed site. Hwang et al. (92) also showed with ^{19}F-^{119}Sn CP MAS NMR that even after calcination, Sn-Beta samples may contain some fluorine that associates with hydrated Sn sites. Recently, hyperpolarization techniques, such as DNP, have been successfully applied to characterize natural abundance ^{119}Sn-Beta samples (93). This technique allows transfer of the polarization from an exogenous biradical containing unpaired electrons to the Sn sites in the sample through the assistance of microwave radiation and a glassing agent. Signal enhancements of approximately 28–75 can be obtained, resulting in an order-of-magnitude decrease in acquisition times. Although the spectra collected via DNP NMR have not generated quantitative data, the accelerated acquisition times allowed
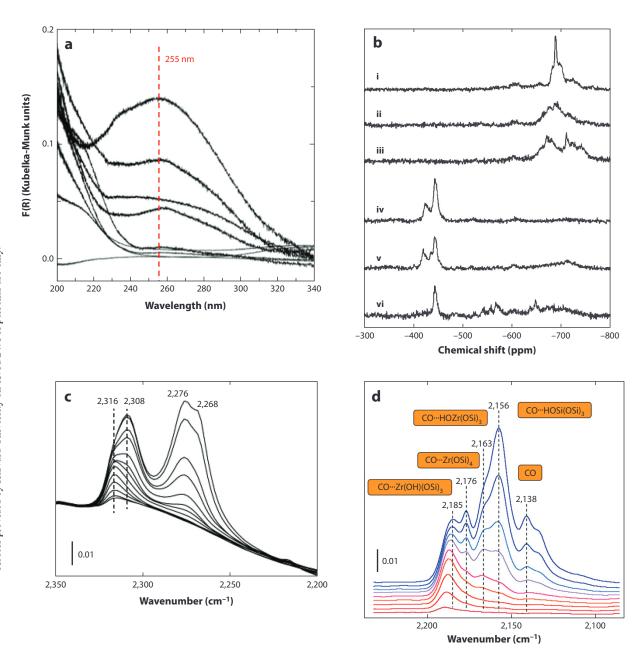
Figure 4

(*a*) Diffuse-reflectance UV (DRUV) spectra of Sn-Beta with varying Sn content (increasing Sn content from bottom to top). The spectra are corrected with a calcined dealuminated zeolite to isolate the Sn-related signals. Reproduced from Dijkmans et al. (88). (*b*) ^{119}Sn magic angle spinning (MAS) solid state NMR spectra of ^{119}Sn-Beta after different treatments: (*i*) calcination, (*ii*) Na exchange, (*iii*) NH$_3$ adsorption, and (*iv–vi*) dehydrated spectra for *i–iii*, respectively. Reproduced from Bermejo-Deval et al. (73). (*c*) Fourier transform infrared spectroscopy (FTIR) spectra at increasing acetonitrile coverage on Sn-Beta. Reproduced from Boronat et al. (67). (*d*) FTIR spectra of CO adsorbed on Zr-Beta collected with increasing CO coverage. Colored boxes show the configuration of adsorption sites assigned to each peak. Reproduced from Sushkevich et al. (69).

Wolf et al. (75) to perform cross-polarization magic-angle turning (CPMAT) experiments to extract important information occluded within the chemical shift anisotropy (CSA). CPMAT experiments correlate the MAS sideband manifolds to a single isotropic chemical shift, allowing the measurement of the CSA for each ^{119}Sn site. The CSA will vary for each site due to the specific anisotropy of the electronic distribution around the Sn nucleus. Thus, the isotropic chemical shift, the span, and the skew were used along with DFT calculations to assign the NMR signals to hydrated open and closed sites (75). Unfortunately, the highly quadrupolar nature of some nuclei, such as Zr and Hf, precludes their analysis with this technique.

X-ray adsorption spectroscopy (XAS) allows the characterization of several Lewis acidic heteroatoms other than Sn to determine, for example, metal coordination quantitatively. However, few experimental studies in the context of Lewis acid zeolite characterization exist because this powerful technique requires X rays generated at a synchrotron facility. For Ti-MFI, the intensity of the 4,967 eV pre-edge peak has been assigned to tetrahedral Ti^{4+}, and its intensity can be used to estimate the fraction of framework Ti atoms (94). EXAFS analysis can also easily distinguish between framework and extraframework sites through detection of M-M scattering interactions. EXAFS may also allow quantitative insight into the connectivity and T-site location of heteroatoms (39, 62, 86). Owing to the low signal-to-noise ratio and extensive modeling required for XAS data analysis, more control studies must be done with various heteroatoms to show conclusive evidence of preferential T-site distributions.

Indirect Detection with Probe Molecules

Probe molecules can be used as an indirect method to assess the local environment of metal centers regardless of the type of heteroatom. In addition, they can be used to compare acidity and reactivity among heteroatoms. Pyridine adsorption coupled with FTIR spectroscopy has been traditionally used to distinguish between Brønsted and Lewis acid sites in zeolites (95–98). However, for most Lewis acid zeolites, bands associated with pyridine-bound Lewis acid centers are not resolved enough to accurately distinguish between framework, extraframework, and nonadsorbing sites. Instead, adsorption of cyclohexanone or deuterated acetonitrile has been extensively used to characterize framework Lewis acid sites with FTIR. Acetonitrile adsorbed on Sn-Beta shows two bands at 2,316 cm^{-1} and 2,308 cm^{-1} that have been attributed to open and closed sites (see **Figure 4c**), respectively, based on DFT predictions (67). However, some reports indicate that these differences could be due to solvent effects of neighboring acetonitrile molecules (99). Other heteroatoms, such as Zr, Hf, and Ti, show only one band in the 2,305–2,315 cm^{-1} range. Sushkevich et al. (69, 100) recently reported that acetonitrile preferentially binds to Zr-Beta open sites and showed that CO adsorption at low temperature ($\sim$100 K) could be used to differentiate between open and closed sites in Zr-Beta (see **Figure 4d**). The bands at 2,185 cm^{-1} and 2,176 cm^{-1} are assigned to CO adsorbed onto the open and closed sites, respectively. As the dosing increases, peaks at 2,156 cm^{-1} and 2,163 cm^{-1} associated with CO adsorbed onto silanol groups and the hydroxy of Zr-OH, respectively, begin to appear. These assignments were further corroborated using OH vibration FTIR and 2,6-di-*tert*-butylpyridine preadsorption experiments. The spectra were deconvoluted with peak fitting to obtain relative amounts of open and closed sites that were shown to vary nonlinearly based on Zr content. This technique could be expanded to probe zeolites containing other heteroatoms to quantify the proportion of open and closed sites.

Akin to FTIR, coupling probe molecule adsorption and NMR spectroscopy can be used to assess acid character and acid site speciation. As highlighted in the section Quantifying Lewis Acidity, Gunther et al. were able to compare the Lewis acidity of various heteroatom-containing zeolites (Sn, Ta, Nb, Zr, Hf, and Ti) using ^{15}N-enriched pyridine (W.R. Gunther, V.K. Michaelis,

R.G. Griffin, and Y. Román-Leshkov, manuscript submitted). This method was able to distinguish framework from extraframework sites and effectively quantify the concentration of framework sites for Sn- and Zr-Beta samples with varying metal content and extraframework content. Lewis acid resonances appear in the range of 260–280 ppm, silanol defect sites feature resonances close to 288 ppm, and extraframework MO_x sites give resonances at 320 ppm. Some of the Lewis acid zeolites, such as Sn- and Ta-Beta, also exhibit a small resonance at 210 ppm indicative of strong Brønsted acid sites. Under hydrated conditions, the resonances for the hydrophobic materials did not change, but the silanol resonances for hydrophilic materials shifted to lower frequency, signifying the replacement of weakly bound pyridine with water. In addition, several of the peaks associated with Lewis acidity were a convolution of multiple resonances, potentially showing the presence of open and closed sites or different populations of T-sites. As mentioned by Dapsens et al. (7), a new opportunity exists in using phosphorus compounds as probe molecules. Due to the 100% abundance of the ^{31}P nuclei, phosphorus NMR can be used for more complex 2D experiments. Trialkylphosphine oxides have already been extensively used to characterize Brønsted acid sites in zeolites (101). Chu et al. (102) have reported a theoretical study in which they correlate the binding strength of trimethylphosphine-Lewis acid (Al, B, Ti) complexes with ^{31}P chemical shift. The broad range of ^{31}P chemical shifts will allow resolving of small changes in Lewis acidity, including the subtle differences between open and closed sites or different T-sites. Unpublished work performed in our group shows uniquely resolved resonances corresponding to different Lewis acid sites in Ti-, Zr-, Hf-, and Sn-Beta zeolites after trimethylphosphine oxide adsorption.

Outlook

As we strive to develop better characterization techniques to probe the various types of sites found in Lewis acid zeolites, it is important to remain vigilant in our interpretation of data. Techniques should provide reproducible results, and reported sample preparation procedures must contain enough detail for others to replicate results. Techniques that detect only MO_x species, such as Raman, direct FTIR, and XRD spectroscopy, should be used with caution, because it is unclear at what concentration extraframework species are first detected. A clear distinction must be made between data that are truly quantitative, data that are semiquantitative, and qualitative trends where numerical comparisons cannot be made. This is especially important for techniques such as NMR, where common methods, such as cross-polarization, will provide quantitative spectra only under very specific analysis conditions (103, 104). For other techniques, such as X-ray photoelectron spectroscopy, that are frequently used to probe substrate-heteroatom interactions but have not been implemented for the analysis of Lewis acid zeolites, it is critical to conduct proper control experiments. We envision that new advances in NMR, probe molecule FTIR, and probe molecule NMR will allow us to reliably quantify differences in T-site distribution and connectivity for zeolite materials containing any Lewis acid heteroatom. Probing the site distribution before and after reaction will help us answer vital questions about catalyst stability and deactivation. Ultimately, we must strive to develop in situ and operando characterization techniques to monitor the evolution and dynamics of sites in real time and under reaction conditions.

STABILITY

Lewis acid zeolites are often used for reaction schemes that involve liquid processing, harsh conditions, and/or the presence of feed impurities. Therefore, catalyst stability is highly important when determining the viability of a zeolite for a particular application. Reversible deactivation can

result from inhibitors that bind to the metal site or oligomeric side products that deposit on the surface or inside the pores. Permanent deactivation can result from loss of crystallinity and porosity in the framework, as well as from leaching of framework heteroatoms. In addition, the connectivity of the Lewis acid center may also evolve under reaction conditions, and it is still unclear whether these changes can be reversed by suitable regeneration techniques. Below, we stress the importance of properly testing for catalyst stability.

Assessing Stability in Batch or Flow

Simple recyclability studies are commonly conducted in the literature to assess the reusability of zeolites for consecutive batch reactions. For these tests, the catalyst is often filtered from the reaction mixture, washed with solvent, and used in a fresh reaction solution. Although a variety of reactions, including MPV reduction and sugar isomerization with M-Beta catalysts, show little deactivation between runs (20, 23, 35, 105), experiments at high turnover numbers must be performed more systematically. For recyclability studies to provide useful information about deactivation, the conditions must be adjusted so that conversion values are never reported at 100% or at thermodynamic equilibrium. Rajabbeigi et al. (106) showed that catalyst deactivation was responsible for the observed concentration plateaus in the isomerization of glucose to fructose in batch reactions. They overcame this problem by adding fresh catalyst to a fresh reaction solution with the same concentration as the previous experiments and repeating this process until there was no additional change in concentration. They were able to use a combination of design of experiments, modeling, and nonlinear parameter estimation to develop a phenomenological model that accounts for the low and high conversion data of glucose to fructose isomerization in water wherein two modes of deactivation exist, namely by the adsorption of side products and by an intrinsic deactivation rate. Indeed, it is important to develop robust methods to characterize deactivation in batch reactions because some industrial processes involve batch or semi-batch reactions. However, although batch methods can provide insight into the reusability of zeolites, flow studies in conjunction with postreaction catalyst characterization are often better suited to assess the long-term stability and deactivation modes for zeolite materials. Unfortunately, very few in-depth flow studies have been conducted with Lewis acid zeolites. Some notable examples are liquid-phase flow studies of Hf-, Zr-, and Sn-Beta zeolites for the transfer hydrogenation and etherification of HMF to produce 2,5-bis(alkoxymethyl)furans (25) and for the MPV reduction of furfural to furfuryl alcohol (107); of Sn-Beta for the conversion of DHA and formaldehyde to HBL (22); of Sn-MFI synthesized by alkali-assisted metalation for the production of glycolic acid from glyoxal (84); and of Sn-MFI, MOR, BEA, and FAU for the isomerization of dihydroxyacetone and xylose (108). The flow study of hydrogenation and etherification of HMF reveals important trends in deactivation that could not have been seen with simple batch reactions (25). Specifically, for reactions using Sn-Beta in ethanol solvent at 393 K, initial transient deactivation from 80% to 60% conversion in the first 10 h time on stream (TOS) is followed by an apparent steady state up to 60 h TOS, which then leads to significant deactivation to below 10% conversion after 100 h TOS (**Figure 5***b*). More details about this study and the mechanisms of deactivation and catalyst characterization are discussed in the section Irreversible Deactivation.
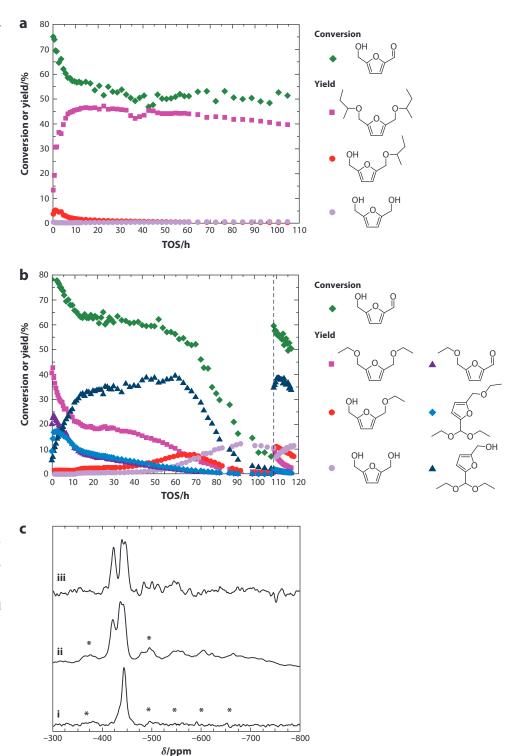
Reversible Deactivation

One of the most common forms of deactivation for catalysts used in liquid-phase biomass conversion processes is the deposition of polymeric species (e.g., humins). The presence of these

Figure 5

(*a*) 5-(Hydroxymethyl)-furfural (HMF) conversion and product yields as a function of time on stream (TOS) for flow reaction with Sn-Beta in 2-butanol. Reaction conditions: 1 wt % HMF, 393 K, 791 kPa, weight hourly space velocity (WHSV) of 3.8 h^{-1}. (*b*) HMF conversion and product yields as a function of TOS for flow reaction with Sn-Beta in ethanol. Reaction conditions: 1 wt % HMF, 393 K, 791 kPa, WHSV of 10.7 h^{-1}. Regeneration of Sn-Beta was performed by calcination at 823 K, designated by the dotted line. (*c*) ^{119}Sn MAS NMR spectra of ^{119}Sn-Beta: (*i*) pristine catalyst; (*ii*) spent catalyst after 96 h TOS under identical conditions as in *b*; (*iii*) same sample as in *ii* but measured with cross polarization [^{119}Sn(^{1}H), $\tau_c = 2$ ms]. The samples were calcined at 823 K prior to analysis. Asterisks mark spinning sidebands. Reproduced from Lewis et al. (25).

organic compounds can be confirmed by thermogravimetric analysis and removed by calcination in air at temperatures higher than 773 K. Materials tested in batch reactors can often recover full original activity with regeneration by calcination, which suggests that deposition of organic species is the main mode of deactivation that is probed in batch reusability studies. Hierarchical zeolites, which possess mesoporosity and reduced diffusion limitations, have been employed to reduce deactivation by coking. Tang et al. (29) found that Zr-Beta with introduced mesoporosity retained constant activity for the ring-opening reaction of styrene oxide with aniline through five recycles, whereas the untreated Zr-Beta lost 75% of its initial activity. In the MPV reduction of furfural with Sn-, Zr-, and Hf-Beta in flow, the major mode of deactivation is the blockage of pores by the polymerization of the product furfuryl alcohol (107). The authors were able to mitigate deactivation by running the reaction at higher temperatures to decrease product adsorption.

An advantage of Lewis acid zeolites is that the metal sites are less susceptible to poisoning by strongly binding species than their homogeneous counterparts. The most common example is the water tolerance of fluoride-synthesized M-Beta zeolites, as mentioned previously in the section Extended Properties. Although water deactivates most homogeneous Lewis acids by strong binding or hydrolysis, water bound to metal centers in Lewis acid zeolites can be reversibly replaced by reactants, akin to the water-stable behavior observed for homogeneous metal triflates with high water exchange rate constants. The reaction of glucose isomerization with Sn-Beta is so resistant to water inhibition that bulk water can be used as the solvent (20). Note that isomerization rates are two times higher in methanol than in water, indicating that the latter solvent is a stronger inhibitor than the former (35, 73). M-Beta zeolites have been shown to retain activity in the presence of water for several reactions, including BV oxidations, MPV reductions, etherifications, and aldol additions (14, 23, 25, 26, 33, 109, 110). Water tolerance is particularly beneficial for cascade reactions, such as the one-pot conversion of furfural to GVL using Zr-Beta and Al-MFI-ns, where certain steps in the process require or produce water. Luo and coworkers (111) showed that GVL yields actually increase from 62% to 68% with the addition of 5 wt% water. The effect of water on reactivity and stability depends on the heteroatom type, the site environment (determined by the zeolite synthesis method), the type of reaction, and the specific solvents and substrates used. Corma et al. (14) found that the Sn-Beta-catalyzed MPV reduction of cyclohexanone in 2-butanol loses more than 80% of its initial activity when 4 wt% water is added to the reaction solution. The resistance to water deactivation followed the order of hydrophobicity: Al-Beta < Sn-Beta < Ti-Beta, which corresponded to the defect concentration of the materials. They found that increasing the hydrophobicity of the material via silylation allowed the material to retain 50% of its activity even with 10 wt% water in the feed. For the coupled MPV reduction and etherification of HMF in ethanol, the addition of 0.2 wt% water decreases the etherification activity of Hf-Beta by 50%, whereas in 2-butanol, the same amount of water has negligible effect on the activity (25).

Lewis acid zeolites are also resistant to other common inhibitors that severely deactivate their homogeneous or grafted analogs. Zhu et al. (23) conducted a study on the effect of acid and base inhibitors on the MPV reduction of 4-tert-butylcyclohexanone and isopropanol with Zr-Beta. They found that although the activity was reduced by up to 30% in the presence of benzoic acid, acetic acid, and pyridine, simply washing with 2-propanol could restore the original activity. Lewis et al. (26) investigated the effect of acetic acid on the aldol condensation of benzaldehyde and acetone with Hf-Beta. Conversion decreased by only 35% upon the addition of 0.11 wt% acetic acid (i.e., a 10:1 acetic acid:Hf molar ratio), and the selectivity to benzalacetone remained high at 93%. Conversely, the solid base catalyst MgO showed negligible activity under the same conditions. Moliner et al. (20) found that glucose isomerization with Sn-Beta exhibits a remarkable resistance to deactivation in strongly acidic solutions by demonstrating that virtually identical fructose yields are obtained using either an HCl solution with pH = 2 or pure water.

Irreversible Deactivation

Structural degradation and metal leaching are common forms of irreversible deactivation for both Brønsted and Lewis acid zeolites. Hydrothermal stability of zeolite frameworks has been well studied for aluminosilicates (112), and many of the conclusions are transferrable to Lewis acidic zeolites. It has been shown that the presence of silanol defect sites is the most significant factor contributing to crystallinity loss during hydrothermal treatments and that hydrophobic materials tend to be more stable (113–116). The structural integrity of Lewis acid zeolites is commonly justified with PXRD patterns that are unchanged after reaction, showing that long-range crystal order is preserved (22, 25, 29, 83). However, PXRD is not able to detect partial pore collapse, which can be quantitatively measured using nitrogen or argon adsorption/desorption. For the conversion of DHA and formaldehyde to HBL using Sn-Beta, a 20% decrease in micropore volume was observed that accounted for a concurrent decrease in HBL yields from 35% to 25%, even after catalyst regeneration by calcination was performed (22). For this study, analysis by PXRD did not show a significant difference in the crystal structure after reaction, thereby providing more concrete evidence that PXRD is not sufficient to exclude structural changes in zeolitic materials.

Incorporation of metal heteroatoms in zeolite frameworks is thermodynamically less stable than the purely siliceous zeolites owing to distortions in bond angles and lengths (13). Therefore, the metal site is especially susceptible to alteration or removal under extreme reaction conditions. Luo et al. (33) showed Sn-MFI nanosheets were resistant to very high thermal treatments at 1,273 K, experiencing no loss in activity for the BV oxidation of 2-adamantanone. However, exposing the material to water at 403 K for 6 h resulted in a 40% decrease in activity. This loss in activity could not be explained by pore collapse alone and most likely resulted from local changes to the metal sites or very limited leaching of the active site. Hot filtration is typically employed to check for metal leaching in a given reaction, and recyclability is used for slightly more extended studies. However, batch reactions typically generate low turnover numbers, because low reagent-to-metal molar ratios are used to speed up results. Consequently, these stability data cannot be extrapolated to extended periods of time. Furthermore, leached metal species may not be active for the desired reaction, which could provide a false negative result. Another diagnostic is to check the metal content of the material or the liquid filtrate, for example, by inductively coupled plasma elemental analysis. However, low metal loading in the Lewis acid zeolites leads to high experimental error, and small changes in metal content may not be detectable. Sádaba et al. (117) provide an excellent tutorial highlighting these issues with a focus on biomass conversion.

Deactivation of Lewis acid zeolite active sites can occur from changes in the local environment and molecular connectivity of the metal center even if no metal loss actually occurs. For example, metal sites may hydrolyze or form extraframework species. Hence, it is imperative to understand the true identity of the active site and how the metal centers evolve under reaction conditions. Work in our group has shown that the local environment of Sn centers in Sn-Beta changes during MPV reduction and etherification of HMF with ethanol, which tracks with a significant drop in etherification activity (25). ^{119}Sn MAS NMR spectra (**Figure 5c**) of calcined samples collected after 96 h on stream under conditions identical to **Figure 5b** show two additional resonances at −436 ppm and −421 ppm when compared to the single resonance at −444 ppm obtained for the pristine catalyst. These additional resonances are indicative of hydrolysis of Sn-O-Si bonds and distortion of the tetrahedral angles, based on more detailed CP experiments of the spent samples. Deuterated acetonitrile FTIR shows a slight red shift of the signal of adsorbed species on tetrahedral Sn sites from 2,309 cm^{-1} to 2,304 cm^{-1} for fresh and postreaction Sn-Beta, respectively, consistent with weakening of the Lewis acid sites for the spent catalyst. In addition, the relative amount of Lewis acid sites to Brønsted acidic hydroxyl groups for the spent catalyst is significantly

lower. It was also shown through ^{13}C NMR and thermogravimetric analysis that ethoxy species form in the zeolite from the reaction of ethanol with silanol groups. This evolution of sites occurs at different rates depending on the heteroatom used; for example, Hf-Beta showed a higher degree of deactivation when compared to Sn-Beta at the same turnover number. Notably, the changes in the site distribution appear to impact the activity for MPV reduction, etherification, and acetalization differently. **Figure 5b** shows that the yields of etherification and acetalization products are higher at lower TOS, but then decrease to less than 5% at longer TOS. In contrast, the yield of the MPV reduction product 5-bis(hydroxymethyl)furan increases at long TOS. Taken together, these data show that the MPV reduction activity is retained despite the decrease in etherification and acetalization activity, thus suggesting that the MPV reduction occurs on different sites or that it can occur on multiple sites, while etherification and acetalization require a specific type of site. Finally, the evolution of sites during reaction strongly depends on the solvent used. When 2-butanol was used instead of ethanol as the solvent (and hydrogen donor), a decrease in activity of <5% was observed at steady state even after 100 h on stream (**Figure 5a**). We hypothesize that the decreased polarity and larger size of 2-butanol compared to ethanol makes it less effective at exchanging onto silanol groups or promoting the hydrolysis of framework bonds. The insights gained from this study into the deactivation modes of M-Beta zeolites show the power of using packed-bed flow reactors combined with detailed catalyst characterization for investigating catalyst stability.

Outlook

The stability of Lewis acid zeolites is an extremely important topic that needs to be addressed more thoroughly in future studies. Not only do the modes of deactivation provide details that relate to the industrial relevance of these materials, but they also provide insight into the nature of catalytically active sites and important steps in the reaction mechanism. We strongly recommend studies in flow mode as the preferred method for investigating catalyst stability and deactivation rates. Characterization of zeolites post-reaction will be of paramount importance for elucidating deactivation mechanisms. An excellent example of this type of study was performed by Lari et al. (108) in which the deactivation of Sn-containing zeolites for the isomerization of dihydroxyacetone and xylose was investigated by coupling fix-bed reactor flow studies with detailed catalyst characterization before and after reaction. A semiquantitative analysis highlighted four main deactivation mechanisms: metal leaching, site restructuring, framework amorphisation, and fouling. Altogether, stability studies on Lewis acid zeolites will increase our understanding of the active sites and will provide critical information for improving the performance of current and new materials.

CONCLUSIONS

Understanding the structure-activity relation of active sites in Lewis acid zeolites is essential for designing materials capable of effectively converting biomass-derived feedstocks. We have shown through numerous examples that catalytic performance depends on several factors, such as heteroatom identity, zeolite framework, and the specific solvent/substrate system. In addition, the wide variation in metal site speciation and the dynamic nature of these sites make it very difficult to establish accurate structure-activity relationships, because site heterogeneity will generate intrinsically different catalytic properties and spectroscopic signatures. Understanding how to measure and control these site distributions is crucial for optimizing and ultimately predicting the catalytic performance of Lewis acid zeolites. We highlight in our outlook sections some of the steps we must take to improve and expand on our current knowledge. Future work should focus on performing

careful kinetic studies to parse out the different contributions of heteroatom identity, zeolitic environment, and substrate/solvent combination to catalytic activity. For these comparisons to be meaningful, it is critical to always establish a benchmark in studies comparing multiple materials, especially ones prepared by postsynthetic techniques, and to normalize rates on a metal content or acid count basis. Reactivity studies should also be coupled with more precise characterization. A major challenge for Lewis acid zeolite spectroscopy is developing reliable methods for probing and quantifying the connectivity of the active site and identifying variations in T-site distribution. It will also be essential to refine detection methods that are applicable for all heteroatoms, such as probe-molecule adsorption. As new characterization techniques are established, it is important to remain vigilant in our interpretation of data and to conduct the proper control experiments. Techniques should provide reproducible results, and a clear distinction must be made between data that are truly quantitative and data that are semiquantitative or qualitative where numerical comparisons cannot be made. The ultimate goal is to develop in situ and operando characterization techniques to monitor the evolution and dynamics of metal sites in real time under reaction conditions. Finally, it is crucial that we perform more long-term stability studies in flow to better understand transient effects and deactivation mechanisms.

DISCLOSURE STATEMENT

The authors are not aware of any affiliations, memberships, funding, or financial holdings that might be perceived as affecting the objectivity of this review.

LITERATURE CITED

1. Taramasso M, Perego G, Notari B. 1983. *Preparation of porous crystalline synthetic material comprised of silicon and titanium oxides.* US Patent No. 7081237
2. Camblor MA, Corma A, Valencia S. 1998. Synthesis in fluoride media and characterisation of aluminosilicate zeolite beta. *J. Mater. Chem.* 8:2137–45
3. Blasco T, Camblor M, Corma A, Esteve P, Guil J, et al. 1998. Direct synthesis and characterization of hydrophobic aluminum-free Ti-beta zeolite. *J. Phys. Chem. B* 102:75–88
4. Taarning E, Osmundsen CM, Yang X, Voss B, Andersen SI, Christensen CH. 2011. Zeolite-catalyzed biomass conversion to fuels and chemicals. *Energy Environ. Sci.* 4:793–804
5. Kubička D, Kubičková I, Čejka J. 2013. Application of molecular sieves in transformations of biomass and biomass-derived feedstocks. *Catal. Rev.* 55:1–78
6. Moliner M. 2014. State of the art of Lewis acid-containing zeolites: lessons from fine chemistry to new biomass transformation processes. *Dalton Trans.* 43:4197–208
7. Dapsens PY, Mondelli C, Pérez-Ramírez J. 2015. Design of Lewis-acid centres in zeolitic matrices for the conversion of renewables. *Chem. Soc. Rev.* 44:7025–43
8. Román-Leshkov Y, Davis ME. 2011. Activation of carbonyl-containing molecules with solid Lewis acids in aqueous media. *ACS Catal.* 1:1566–80
9. Gounder R, Davis ME. 2013. Beyond shape selective catalysis with zeolites: Hydrophobic void spaces in zeolites enable catalysis in liquid water. *AIChE J.* 59:3349–58
10. Boronat M, Corma A, Renz M, Viruela PM. 2006. Predicting the activity of single isolated Lewis acid sites in solid catalysts. *Chem. A Eur. J.* 12:7067–77
11. Yang G, Zhou L, Han X. 2012. Lewis and Brönsted acidic sites in M^{4+}-doped zeolites (M = Ti, Zr, Ge, Sn, Pb) as well as interactions with probe molecules: a DFT study. *J. Mol. Catal. A Chem.* 363:371–79
12. Li Y-P, Head-Gordon M, Bell AT. 2014. Analysis of the reaction mechanism and catalytic activity of metal-substituted beta zeolite for the isomerization of glucose to fructose. *ACS Catal.* 4:1537–45
13. Yang G, Pidko EA, Hensen EJ. 2013. Structure, stability, and Lewis acidity of mono and double Ti, Zr, and Sn framework substitutions in BEA zeolites: a periodic density functional theory study. *J. Phys. Chem. C* 117:3976–86

14. Corma A, Domine ME, Valencia S. 2003. Water-resistant solid Lewis acid catalysts: Meerwein–Ponndorf–Verley and Oppenauer reactions catalyzed by tin-beta zeolite. *J. Catal.* 215:294–304

15. Li H, Wang J, Zhou D, Tian D, Shi C, et al. 2015. Structural stability and Lewis acidity of tetravalent Ti, Sn, or Zr-linked interlayer-expanded zeolite COE-4: a DFT study. *Microporous Mesoporous Mater.* 218:160–66

16. Shetty S, Kulkarni BS, Kanhere DG, Goursot A, Pal S. 2008. A comparative study of structural, acidic and hydrophilic properties of Sn-BEA with Ti-BEA using periodic density functional theory. *J. Phys. Chem. B* 112:2573–79

17. Kulkarni BS, Krishnamurty S, Pal S. 2010. Probing Lewis acidity and reactivity of Sn- and Ti-beta zeolite using industrially important moieties: a periodic density functional study. *J. Mol. Catal. A Chem.* 329:36–43

18. van der Waal JC, Rigutto MS, van Bekkum H. 1998. Zeolite titanium beta as a selective catalyst in the epoxidation of bulky alkenes. *Appl. Catal. A Gen.* 167:331–42

19. van der Waal JC, van Bekkum H. 1997. Zeolite titanium beta: a versatile epoxidation catalyst. Solvent effects. *J. Mol. Catal. A Chem.* 124:137–46

20. Moliner M, Román-Leshkov Y, Davis ME. 2010. Tin-containing zeolites are highly active catalysts for the isomerization of glucose in water. *PNAS* 107:6164–68

21. Wolf P, Hammond C, Conrad S, Hermans I. 2014. Post-synthetic preparation of Sn-, Ti- and Zr-beta: a facile route to water tolerant, highly active Lewis acidic zeolites. *Dalton Trans.* 43:4514–19

22. Van de Vyver S, Odermatt C, Romero K, Prasomsri T, Román-Leshkov Y. 2015. Solid Lewis acids catalyze the carbon–carbon coupling between carbohydrates and formaldehyde. *ACS Catal.* 5:972–77

23. Zhu Y, Chuah G, Jaenicke S. 2004. Chemo- and regioselective Meerwein–Ponndorf–Verley and Oppenauer reactions catalyzed by Al-free Zr-zeolite beta. *J. Catal.* 227:1–10

24. Luo HY, Consoli DF, Gunther WR, Román-Leshkov Y. 2014. Investigation of the reaction kinetics of isolated Lewis acid sites in beta zeolites for the Meerwein–Ponndorf–Verley reduction of methyl levulinate to γ-valerolactone. *J. Catal.* 320:198–207

25. Lewis JD, Van de Vyver S, Crisci AJ, Gunther WR, Michaelis VK, et al. 2014. A continuous flow strategy for the coupled transfer hydrogenation and etherification of 5-(hydroxymethyl) furfural using Lewis acid zeolites. *ChemSusChem* 7:2255–65

26. Lewis JD, Van de Vyver S, Román-Leshkov Y. 2015. Acid–base pairs in Lewis acidic zeolites promote direct aldol reactions by soft enolization. *Angew. Chem. Int. Ed.* 54:9835–38

27. Corma A. 1997. From microporous to mesoporous molecular sieve materials and their use in catalysis. *Chem. Rev.* 97:2373–420

28. Dapsens PY, Mondelli C, Jagielski J, Hauert R, Pérez-Ramírez J. 2014. Hierarchical Sn-MFI zeolites prepared by facile top-down methods for sugar isomerisation. *Catal. Sci. Technol.* 4:2302–11

29. Tang B, Dai W, Sun X, Wu G, Guan N, et al. 2015. Mesoporous Zr-Beta zeolites prepared by a post-synthetic strategy as a robust Lewis acid catalyst for the ring-opening aminolysis of epoxides. *Green Chem.* 17:1744–55

30. Kumar M, Luo H, Román-Leshkov Y, Rimer JD. 2015. SSZ-13 crystallization by particle attachment and deterministic pathways to crystal size control. *J. Am. Chem. Soc.* 137:13007–17

31. Lupulescu AI, Kumar M, Rimer JD. 2013. A facile strategy to design zeolite L crystals with tunable morphology and surface architecture. *J. Am. Chem. Soc.* 135:6608–17

32. Ouyang X, Hwang S-J, Xie D, Rea T, Zones SI, Katz A. 2015. Heteroatom-substituted delaminated zeolites as solid Lewis acid catalysts. *ACS Catal.* 5:3108–19

33. Luo HY, Bui L, Gunther WR, Min E, Román-Leshkov Y. 2012. Synthesis and catalytic activity of Sn-MFI nanosheets for the Baeyer–Villiger oxidation of cyclic ketones. *ACS Catal.* 2:2695–99

34. Ren L, Guo Q, Kumar P, Orazov M, Xu D, et al. 2015. Self-pillared, single-unit-cell Sn-MFI zeolite nanosheets and their use for glucose and lactose isomerization. *Angew. Chem. Int. Ed.* 54:10848–51

35. Gounder R, Davis ME. 2013. Monosaccharide and disaccharide isomerization over Lewis acid sites in hydrophobic and hydrophilic molecular sieves. *J. Catal.* 308:176–88

36. Bai P, Siepmann JI, Deem MW. 2013. Adsorption of glucose into zeolite beta from aqueous solution. *AIChE J.* 59:3523–29

37. Sastre G, Corma A. 1999. Relation between structure and Lewis acidity of Ti-Beta and TS-1 zeolites: a quantum-chemical study. *Chem. Phys. Lett.* 302:447–53

38. Shetty S, Pal S, Kanhere DG, Goursot A. 2006. Structural, electronic, and bonding properties of zeolite Sn-beta: a periodic density functional theory study. *Chem. A Eur. J.* 12:518–23

39. Bare SR, Kelly SD, Sinkler W, Low JJ, Modica FS, et al. 2005. Uniform catalytic site in Sn-β-zeolite determined using x-ray absorption fine structure. *J. Am. Chem. Soc.* 127:12924–32

40. Newsam J, Treacy MM, Koetsier W, De Gruyter C. 1988. Structural characterization of zeolite beta. *Proc. R. Soc. Lond. A Math. Phys. Sci.* 420:375–405

41. Baerlocher C, McCusker LB, Olson DH. 2007. *Atlas of Zeolite Framework Types*. London: Elsevier

42. Yuan S, Si H, Fu A, Chu T, Tian F, et al. 2011. Location of Si vacancies and [Ti (OSi) 4] and [Ti (OSi) 3OH] sites in the MFI framework: a large cluster and full ab initio study. *J. Phys. Chem. A* 115:940–47

43. Millini R, Perego G, Seiti K. 1994. Ti substitution in MFI type zeolites: a quantum mechanical study. *Stud. Surf. Sci. Catal.* 84:2123–29

44. Oumi Y, Matsuba K, Kubo M, Inui T, Miyamoto A. 1995. Selective T-site substitution as a cause of the anisotropy of lattice expansion in titanosilicate-1 investigated by molecular dynamics and computer graphics. *Microporous Mater.* 4:53–57

45. Njo SL, van Koningsveld H, van de Graaf B. 1997. A combination of the Monte Carlo method and molecular mechanics calculations: a novel way to study the Ti (IV) distribution in titanium silicalite-1. *J. Phys. Chem. B* 101:10065–68

46. Ricchiardi G, de Man A, Sauer J. 2000. The effect of hydration on structure and location of Ti-sites in Ti-silicalite catalysts. A computational study. *Phys. Chem. Chem. Phys.* 2:2195–204

47. Atoguchi T, Yao S. 2003. Ti atom in MFI zeolite framework: a large cluster model study by ONIOM method. *J. Mol. Catal. A Chem.* 191:281–88

48. Gamba A, Tabacchi G, Fois E. 2009. TS-1 from first principles. *J. Phys. Chem. A* 113:15006–15

49. Deka RC, Nasluzov VA, Ivanova Shor EA, Shor AM, Vayssilov GN, Rösch N. 2005. Comparison of all sites for Ti substitution in zeolite TS-1 by an accurate embedded-cluster method. *J. Phys. Chem. B* 109:24304–10

50. Hijar C, Jacubinas R, Eckert J, Henson N, Hay P, Ott K. 2000. The siting of Ti in TS-1 is non-random. Powder neutron diffraction studies and theoretical calculations of TS-1 and FeS-1. *J. Phys. Chem. B* 104:12157–64

51. Lamberti C, Bordiga S, Zecchina A, Artioli G, Marra G, Spano G. 2001. Ti location in the MFI framework of Ti-silicalite-1: a neutron powder diffraction study. *J. Am. Chem. Soc.* 123:2204–12

52. Henry PF, Weller MT, Wilson CC. 2001. Structural investigation of TS-1: determination of the true nonrandom titanium framework substitution and silicon vacancy distribution from powder neutron diffraction studies using isotopes. *J. Phys. Chem. B* 105:7452–58

53. Lamberti C, Bordiga S, Zecchina A, Carati A, Fitch A, et al. 1999. Structural characterization of Ti-silicalite-1: a synchrotron radiation X-ray powder diffraction study. *J. Catal.* 183:222–31

54. Marra G, Artioli G, Fitch A, Milanesio M, Lamberti C. 2000. Orthorhombic to monoclinic phase transition in high-Ti-loaded TS-1: an attempt to locate Ti in the MFI framework by low temperature XRD. *Microporous Mesoporous Mater.* 40:85–94

55. Conrad S, Verel R, Hammond C, Wolf P, Göltl F, Hermans I. 2015. Silica-grafted Sn^{IV} catalysts in hydrogen-transfer reactions. *ChemCatChem* 7:3270–78

56. Boronat M, Concepción P, Corma A, Navarro MT, Renz M, Valencia S. 2009. Reactivity in the confined spaces of zeolites: the interplay between spectroscopy and theory to develop structure–activity relationships for catalysis. *Phys. Chem. Chem. Phys.* 11:2876–84

57. Corma A, Navarro MT, Renz M. 2003. Lewis acidic Sn (IV) centers—grafted onto MCM-41—as catalytic sites for the Baeyer–Villiger oxidation with hydrogen peroxide. *J. Catal.* 219:242–46

58. Osmundsen CM, Holm MS, Dahl S, Taarning E. 2012. Tin-containing silicates: structure–activity relations. *Proc. R. Soc. Lond. A Math. Phys. Sci.* 468:2000–16

59. Cho HJ, Dornath P, Fan W. 2014. Synthesis of hierarchical Sn-MFI as Lewis acid catalysts for isomerization of cellulosic sugars. *ACS Catal.* 4:2029–37

60. De Clercq R, Dusselier M, Christiaens C, Dijkmans J, Iacobescu RI, et al. 2015. Confinement effects in Lewis acid catalyzed sugar conversion: steering toward functional polyester building blocks. *ACS Catal.* 5:5803–11

61. Lew CM, Rajabbeigi N, Tsapatsis M. 2012. Tin-containing zeolite for the isomerization of cellulosic sugars. *Microporous Mesoporous Mater.* 153:55–58

62. Gleeson D, Sankar G, Catlow CRA, Thomas JM, Spanó G, et al. 2000. The architecture of catalytically active centers in titanosilicate (TS-1) and related selective-oxidation catalysts. *Phys. Chem. Chem. Phys.* 2:4812–17

63. Bermejo-Deval R, Assary RS, Nikolla E, Moliner M, Román-Leshkov Y, et al. 2012. Metalloenzyme-like catalyzed isomerizations of sugars by Lewis acid zeolites. *PNAS* 109:9727–32

64. Wells DH, Delgass WN, Thomson KT. 2004. Evidence of defect-promoted reactivity for epoxidation of propylene in titanosilicate (TS-1) catalysts: a DFT study. *J. Am. Chem. Soc.* 126:2956–62

65. Khouw CB, Davis ME. 1995. Catalytic activity of titanium silicates synthesized in the presence of alkali-metal and alkaline-earth ions. *J. Catal.* 151:77–86

66. Bordiga S, Bonino F, Damin A, Lamberti C. 2007. Reactivity of Ti(IV) species hosted in TS-1 to-wards H_2O_2–H_2O solutions investigated by ab initio cluster and periodic approaches combined with experimental XANES and EXAFS data: a review and new highlights. *Phys. Chem. Chem. Phys.* 9:4854–78

67. Boronat M, Concepción P, Corma A, Renz M, Valencia S. 2005. Determination of the catalytically active oxidation Lewis acid sites in Sn-beta zeolites, and their optimisation by the combination of theoretical and experimental studies. *J. Catal.* 234:111–18

68. Boronat M, Corma A, Renz M. 2006. Mechanism of the Meerwein-Ponndorf-Verley-Oppenauer (MPVO) redox equilibrium on Sn-and Zr-beta zeolite catalysts. *J. Phys. Chem. B* 110:21168–74

69. Sushkevich VL, Palagin D, Ivanova II. 2015. With open arms: open sites of ZrBEA zeolite facilitate selective synthesis of butadiene from ethanol. *ACS Catal.* 5:4833–36

70. Román-Leshkov Y, Moliner M, Labinger JA, Davis ME. 2010. Mechanism of glucose isomerization using a solid Lewis acid catalyst in water. *Angew. Chem. Int. Ed.* 49:8954–57

71. Gunther WR, Wang Y, Ji Y, Michaelis VK, Hunt ST, et al. 2012. Sn-Beta zeolites with borate salts catalyse the epimerization of carbohydrates via an intramolecular carbon shift. *Nat. Commun.* 3:1109

72. Gunther WR, Duong Q, Román-Leshkov Y. 2013. Catalytic consequences of borate complexation and pH on the epimerization of L-arabinose to L-ribose in water catalyzed by Sn-Beta zeolite with borate salts. *J. Mol. Catal. A Chem.* 379:294–302

73. Bermejo-Deval R, Orazov M, Gounder R, Hwang S-J, Davis ME. 2014. Active sites in Sn-beta for glucose isomerization to fructose and epimerization to mannose. *ACS Catal.* 4:2288–97

74. Brand SK, Labinger JA, Davis ME. 2015. Tin silsesquioxanes as models for the "open" site in tin-containing zeolite Beta. *ChemCatChem* 8:121–24

75. Wolf P, Valla M, Rossini AJ, Comas-Vives A, Núñez-Zarur F, et al. 2014. NMR signatures of the active sites in Sn-β zeolite. *Angew. Chem.* 126:10343–47

76. Zimmerman PM, Head-Gordon M, Bell AT. 2011. Selection and validation of charge and Lennard-Jones parameters for QM/MM simulations of hydrocarbon interactions with zeolites. *J. Chem. Theory Comput.* 7:1695–703

77. Rai N, Caratzoulas S, Vlachos DG. 2013. Role of silanol group in Sn-beta zeolite for glucose isomerization and epimerization reactions. *ACS Catal.* 3:2294–98

78. Li G, Pidko EA, Hensen EJ. 2014. Synergy between Lewis acid sites and hydroxyl groups for the isomerization of glucose to fructose over Sn-containing zeolites: a theoretical perspective. *Catal. Sci. Technol.* 4:2241–50

79. Tolborg S, Katerinopoulou A, Falcone DD, Sádaba I, Osmundsen CM, et al. 2014. Incorporation of tin affects crystallization, morphology, and crystal composition of Sn-Beta. *J. Mater. Chem. A* 2:20252–62

80. Wakihara T, Iida T, Okubo T, Kohara S, Takagaki A. 2015. Sn-beta zeolite catalysts with high Sn contents prepared from Sn-Si mixed oxide composites. *ChemNanoMat* 1:155–58

81. Hammond C, Conrad S, Hermans I. 2012. Simple and scalable preparation of highly active Lewis acidic Sn-β. *Angew. Chem. Int. Ed.* 51:11736–39

82. Chang C-C, Cho HJ, Wang Z, Wang X, Fan W. 2015. Fluoride-free synthesis of a Sn-BEA catalyst by dry gel conversion. *Green Chem.* 17:2943–51

83. Tang B, Dai W, Wu G, Guan N, Li L, Hunger M. 2014. Improved postsynthesis strategy to Sn-Beta zeolites as Lewis acid catalysts for the ring-opening hydration of epoxides. *ACS Catal.* 4:2801–10

84. Dapsens PY, Mondelli C, Kusema BT, Verel R, Pérez-Ramírez J. 2014. A continuous process for glyoxal valorisation using tailored Lewis-acid zeolite catalysts. *Green Chem.* 16:1176–86

85. van der Graaff WN, Li G, Mezari B, Pidko EA, Hensen EJ. 2015. Synthesis of Sn-Beta with exclusive and high framework Sn content. *ChemCatChem* 7:1152–60

86. Hammond C, Padovan D, Al-Nayili A, Wells P, Gibson EK, Dimitratos N. 2015. Identification of active and spectator Sn sites in Sn-β following solid-state stannation, and consequences for Lewis acid catalysis. *ChemCatChem* 7:3322–31

87. van Bokhoven JA, Koningsberger DC, Kunkeler P, van Bekkum H, Kentgens APM. 2000. Stepwise dealumination of zeolite Beta at specific T-sites observed with ^{27}Al MAS and ^{27}Al MQ MAS NMR. *J. Am. Chem. Soc.* 122:12842–47

88. Dijkmans J, Demol J, Houthoofd K, Huang S, Pontikes Y, Sels B. 2015. Post-synthesis Snβ: an exploration of synthesis parameters and catalysis. *J. Catal.* 330:545–57

89. Dijkmans J, Dusselier M, Janssens W, Trekels M, Vantomme A, et al. 2016. An inner-/outer-sphere stabilized Sn active site in β-zeolite: spectroscopic evidence and kinetic consequences. *ACS Catal.* 6:31–46

90. Bermejo-Deval R, Gounder R, Davis ME. 2012. Framework and extraframework tin sites in zeolite Beta react glucose differently. *ACS Catal.* 2:2705–13

91. Dartt C, Khouw C, Li H-X, Davis M. 1994. Synthesis and physicochemical properties of zeolites containing framework titanium. *Microporous Mater.* 2:425–37

92. Hwang S-J, Gounder R, Bhawe Y, Orazov M, Bermejo-Deval R, Davis ME. 2015. Solid state NMR characterization of Sn-Beta zeolites that catalyze glucose isomerization and epimerization. *Topics Catal.* 58:435–40

93. Gunther WR, Michaelis VK, Caporini MA, Griffin RG, Román-Leshkov Y. 2014. Dynamic nuclear polarization NMR enables the analysis of Sn-Beta zeolite prepared with natural abundance ^{119}Sn precursors. *J. Am. Chem. Soc.* 136:6219–22

94. Ricchiardi G, Damin A, Bordiga S, Lamberti C, Spanò G, et al. 2001. Vibrational structure of titanium silicate catalysts. A spectroscopic and theoretical study. *J. Am. Chem. Soc.* 123:11409–19

95. Buzzoni R, Bordiga S, Ricchiardi G, Lamberti C, Zecchina A, Bellussi G. 1996. Interaction of pyridine with acidic (H-ZSm5, H-β, H-Mord zeolites) and superacidic (H-nafion membrane) systems: an IR investigation. *Langmuir* 12:930–40

96. Emeis C. 1993. Determination of integrated molar extinction coefficients for infrared absorption bands of pyridine adsorbed on solid acid catalysts. *J. Catal.* 141:347–54

97. Barzetti T, Selli E, Moscotti D, Forni L. 1996. Pyridine and ammonia as probes for FTIR analysis of solid acid catalysts. *J. Chem. Soc. Faraday Trans.* 92:1401–7

98. Farneth W, Gorte R. 1995. Methods for characterizing zeolite acidity. *Chem. Rev.* 95:615–35

99. Roy S, Bakhmutsky K, Mahmoud E, Lobo RF, Gorte RJ. 2013. Probing Lewis acid sites in Sn-Beta zeolite. *ACS Catal.* 3:573–80

100. Sushkevich VL, Vimont A, Travert A, Ivanova II. 2015. Spectroscopic evidence for open and closed Lewis acid sites in ZrBEA zeolites. *J. Phys. Chem. C* 119:17633–39

101. Zheng A, Huang S-J, Liu S-B, Deng F. 2011. Acid properties of solid acid catalysts characterized by solid-state ^{31}P NMR of adsorbed phosphorous probe molecules. *Phys. Chem. Chem. Phys.* 13:14889–901

102. Chu Y, Yu Z, Zheng A, Fang H, Zhang H, et al. 2011. Acidic strengths of Brønsted and Lewis acid sites in solid acids scaled by ^{31}P NMR chemical shifts of adsorbed trimethylphosphine. *J. Phys. Chem. C* 115:7660–67

103. Johnson RL, Schmidt-Rohr K. 2014. Quantitative solid-state ^{13}C NMR with signal enhancement by multiple cross polarization. *J. Magn. Reson.* 239:44–49

104. Offerdahl TJ, Salsbury JS, Dong Z, Grant DJ, Schroeder SA, et al. 2005. Quantitation of crystalline and amorphous forms of anhydrous neotame using ^{13}C CPMAS NMR spectroscopy. *J. Pharm. Sci.* 94:2591–605

105. Guo Q, Fan F, Pidko EA, van der Graaff WN, Feng Z, et al. 2013. Highly active and recyclable Sn-MWW zeolite catalyst for sugar conversion to methyl lactate and lactic acid. *ChemSusChem* 6:1352–56

106. Rajabbeigi N, Torres A, Lew C, Elyassi B, Ren L, et al. 2014. On the kinetics of the isomerization of glucose to fructose using Sn-Beta. *Chem. Eng. Sci.* 116:235–42

107. Koehle M, Lobo RF. 2015. Lewis acidic zeolite Beta catalyst for the Meerwein-Ponndorf-Verley reduction of furfural. *Catal. Sci. Technol.* In press. doi: 10.1039/c5cy01501d

108. Lari GM, Dapsens PY, Scholz D, Mitchell S, Mondelli C, Péréz-Ramírez J. 2016. Deactivation mechanisms of tin-zeolites in biomass conversions. *Green Chem.* 18:1249–60

109. Corma A, Llabrés i Xamena FX, Prestipino C, Renz M, Valencia S. 2009. Water resistant, catalytically active Nb and Ta isolated Lewis acid sites, homogeneously distributed by direct synthesis in a Beta zeolite. *J. Phys. Chem. C* 113:11306–15

110. Corma A, Nemeth LT, Renz M, Valencia S. 2001. Sn-zeolite beta as a heterogeneous chemoselective catalyst for Baeyer–Villiger oxidations. *Nature* 412:423–25

111. Bui L, Luo H, Gunther WR, Román-Leshkov Y. 2013. Domino reaction catalyzed by zeolites with Brønsted and Lewis acid sites for the production of γ-valerolactone from furfural. *Angew. Chem.* 125:8180–83

112. Beyerlein R, Choi-Feng C, Hall J, Huggins B, Ray G. 1997. Effect of steaming on the defect structure and acid catalysis of protonated zeolites. *Top. Catal.* 4:27–42

113. Zhang L, Chen K, Chen B, White JL, Resasco DE. 2015. Factors that determine zeolite stability in hot liquid water. *J. Am. Chem. Soc.* 137:11810–19

114. Zapata PA, Huang Y, Gonzalez-Borja MA, Resasco DE. 2013. Silylated hydrophobic zeolites with enhanced tolerance to hot liquid water. *J. Catal.* 308:82–97

115. Vjunov A, Derewinski MA, Fulton JL, Camaioni DM, Lercher JA. 2015. Impact of zeolite aging in hot liquid water on activity for acid-catalyzed dehydration of alcohols. *J. Am. Chem. Soc.* 137:10374–82

116. Vjunov A, Fulton JL, Camaioni DM, Hu JZ, Burton SD, et al. 2015. Impact of aqueous medium on zeolite framework integrity. *Chem. Mater.* 27:3533–45

117. Sádaba I, Granados ML, Riisager A, Taarning E. 2015. Deactivation of solid catalysts in liquid media: the case of leaching of active sites in biomass conversion reactions. *Green Chem.* 17:4133–45

118. Taarning E, Saravanamurugan S, Spangsberg Holm M, Xiong J, West RM, Christensen CH. 2009. Zeolite-catalyzed isomerization of triose sugars. *ChemSusChem* 2:625–27

119. Corma A, Domine ME, Nemeth L, Valencia S. 2002. Al-free Sn-Beta zeolite as a catalyst for the selective reduction of carbonyl compounds (Meerwein-Ponndorf-Verley reaction). *J. Am. Chem. Soc.* 124:3194–95

120. Sushkevich VL, Ivanova II, Tolborg S, Taarning E. 2014. Meerwein–Ponndorf–Verley–Oppenauer reaction of crotonaldehyde with ethanol over Zr-containing catalysts. *J. Catal.* 316:121–29

121. Li L, Cani D, Pescarmona PP. 2015. Metal-containing TUD-1 mesoporous silicates as versatile solid acid catalysts for the conversion of bio-based compounds into valuable chemicals. *Inorg. Chim. Acta* 431:289–96

122. Pacheco JJ, Davis ME. 2014. Synthesis of terephthalic acid via Diels-Alder reactions with ethylene and oxidized variants of 5-hydroxymethylfurfural. *PNAS* 111:8363–67

123. Mal NK, Ramaswamy AV. 1996. Hydroxylation of phenol over Sn-silicalite-1 molecular sieve: solvent effects. *J. Mol. Catal. A Chem.* 105:149–58

124. Bhagwat M, Shah P, Ramaswamy V. 2003. Synthesis of nanocrystalline SnO_2 powder by amorphous citrate route. *Mater. Lett.* 57:1604–11

125. Dijkmans J, Dusselier M, Gabriëls D, Houthoofd K, Magusin PCMM, et al. 2015. Cooperative catalysis for multistep biomass conversion with Sn/Al Beta zeolite. *ACS Catal.* 5:928–40

126. Pang G, Chen S, Koltypin Y, Zaban A, Feng S, Gedanken A. 2001. Controlling the particle size of calcined SnO_2 nanocrystals. *Nano Lett.* 1:723–26

127. Chaudhari K, Das T, Rajmohanan P, Lazar K, Sivasanker S, Chandwadkar A. 1999. Synthesis, characterization, and catalytic properties of mesoporous tin-containing analogs of MCM-41. *J. Catal.* 183:281–91

128. Li L, Collard X, Bertrand A, Sels BF, Pescarmona PP, Aprile C. 2014. Extra-small porous Sn-silicate nanoparticles as catalysts for the synthesis of lactates. *J. Catal.* 314:56–65

129. Mal N, Ramaswamy V, Rajamohanan P, Ramaswamy A. 1997. Sn-MFI molecular sieves: synthesis methods, ^{29}Si liquid and solid MAS-NMR, ^{119}Sn static and MAS NMR studies. *Microporous Mater.* 12:331–40

130. Casagrande M, Moretti E, Storaro L, Lenarda M, Gersich J, et al. 2006. Synthesis and structural charac-
terization of MSU-type silica–tin molecular sieves: post-synthesis grafting of tin chlorides. *Microporous
Mesoporous Mater.* 91:261–67

131. Lázár K, Szeleczky A, Mal N, Ramaswamy A. 1997. In situ [119]Sn-Mössbauer spectroscopic study on
MR, MEL, and MTW tin silicalites. *Zeolites* 19:123–27

132. Lazar K, Chandwadkar A, Fejes P, Čejka J, Ramaswamy A. 2000. Valency changes of iron and tin in
framework-substituted molecular sieves investigated by in situ Mössbauer spectroscopy. *J. Radioanal.
Nuclear Chem.* 246:143–48

133. Özkendir O, Ufuktepe Y. 2007. Electronic and structural properties of SnO and SnO_2 thin films studied
by X-ray-absorption spectroscopy. *J. Optoelectron. Adv. Mater.* 9:3729–33

134. Nemeth L, Moscoso J, Erdman N, Bare S, Oroskar A, et al. 2004. Synthesis and characterization of
Sn-Beta as a selective oxidation catalyst. *Stud. Surf. Sci. Catal.* 154:2626–31

135. Antunes MM, Lima S, Neves P, Magalhães AL, Fazio E, et al. 2015. One-pot conversion of furfural to
useful bio-products in the presence of a Sn, Al-containing zeolite beta catalyst prepared via post-synthesis
routes. *J. Catal.* 329:522–37

136. Courtney TD, Chang C-C, Gorte RJ, Lobo RF, Fan W, Nikolakis V. 2015. Effect of water treatment
on Sn-BEA zeolite: origin of 960 cm^{-1} FTIR peak. *Microporous Mesoporous Mater.* 210:69–76

137. Dijkmans J, Gabriëls D, Dusselier M, de Clippel F, Vanelderen P, et al. 2013. Productive sugar isomer-
ization with highly active Sn in dealuminated β zeolites. *Green Chem.* 15:2777–85

138. Zhuang J, Han X, Bao X. 2015. In-situ ^{31}P MAS NMR probing of the active centers in Ti silicalite
molecular sieve. *Catal. Commun.* 62:75–78

139. Renz M, Blasco T, Corma A, Fornés V, Jensen R, Nemeth L. 2002. Selective and shape-selective Baeyer–
Villiger oxidations of aromatic aldehydes and cyclic ketones with Sn-Beta zeolites and H_2O_2. *Chem. A
Eur. J.* 8:4708–17

Contents

Indexes

Errata

An online log of corrections to *Annual Review of Chemical and Biomolecular Engineering*
articles may be found at http://www.annualreviews.org/errata/chembioeng